

2

THE FLORIDA STATE UNIVERSITY
Tallahassee, Florida 32306-3034

AD-A253 182



DTIC
ELECTE
JUL 22 1992
S C D



FINAL TECHNICAL REPORT

Air-Sea Interaction in Regions of Varying Surface Conditions

ONR Contract N00014-89-J-1660

July 1992

Signed:


Steven A. Stage
Associate Professor
Department of Meteorology
Florida State University
Tallahassee, Florida
Principal Investigator
Telephone (904) 644-2037


DISTRIBUTION STATEMENT A

Approved for public release;
Distribution Unlimited

92 7 1 094

92-19024



1. Introduction

The Frontal Air-Sea Interaction Experiment (FASINEX) was a field experiment that was primarily performed in the Fall of 1985 and Spring of 1986 in the vicinity of the subtropical oceanic front south of Bermuda (Stage and Weller, 1985). Leadership and primary funding for this experiment came from the Office of Naval Research (ONR) with additional funding for some participants coming from several other governmental agencies including NSF, NASA, and NOAA. FASINEX arose from the realization that little data was available about atmospheric and oceanic processes in regions of non-homogeneous sea surface temperature (SST) such as the subtropical SST front south of Bermuda. What data was available indicated that such regions behave significantly differently than homogeneous areas. A more complete discussion of the scientific motivation and objectives for FASINEX can be found in Stage and Weller (1985) and the experimental field plan in Stage and Weller (1986).

This is a final report on the work done at The Florida State University (FSU) as a part of FASINEX under contract number N00014-89-J-1660 titled Air-Sea Interaction in Regions of Varying Surface Conditions. This work is a continuation of previous research done under ONR support and involves considerable overlap.

2. Project Goals

The chief goal of this project was to develop an understanding of the behavior of the Marine Atmospheric Boundary Layer (MABL) in the vicinity of the FASINEX SST front. There were two major components to this work:

- A. To study turbulent fluxes and other turbulent statistics in the vicinity of the SST front as measured by FASINEX aircraft. Special statistical methods were devised and used to show how these quantities change near the SST front.
- B. To study the structure of the MABL in by analysis of results from a two dimensional numerical model. MABL structure was examined as a function of the direction of the synoptic scale geostrophic wind relative to the front. We also looked at the secondary circulations induced in the MABL by the SST front.

3. Project Accomplishments

3.1. Turbulent fluxes near the SST front.

One of the goals of this project was to determine how the turbulent fluxes, variances, and covariances change in the vicinity of the FASINEX SST front. An important question that arises in this non-homogeneous region is how to go about computing these statistics. Traditional Reynolds fluxes are computed in homogeneous conditions by taking time signals, removing long term variations by high pass filtering or linear trend removal and then computing the variances and covariances. Authors differ in the high pass filters used and in the averaging time used in computing the variances and covariances. In non-homogeneous situations these issues become crucial to meaningful interpretation of the data. In homogeneous situations, too short an averaging time results in statistics that do not include all of the important scales of motion and that are subject to high stochastic variability and uncertainty due to an insufficient number of cycles of the significant frequencies. Longer averaging reduces these effects but introduces variance and covariance that is associated with mesoscale or synoptic scale processes. In non-homogeneous cases these same concerns are relevant plus there is the added problem that longer averaging has the undesirable effect of smearing out the changes in turbulent statistics at the front and thus hiding the sharpness of the changes there.

Crescenti (1988) has devised two methods for computing turbulent fluxes, variances, and covariances that faces these problems. The methods consist of computing statistics that depend on position rather than the traditional method of computing a single value. In the first method a

boxcar running mean filter is applied to the data. Data within the boxcar is linearly detrended and variances and covariances are computed over the length of the boxcar. This technique has the advantage that the value computed is the same as would be found by breaking the data into a block with the same length as the boxcar. It also preserves the usual mathematical properties needed to achieve Reynolds decomposition of the atmospheric budget equations. The second method consists of using an FFT to perform a sharp high pass filter on the data, multiplying the resulting signals and using an FFT-based low pass filter to perform the averaging needed to compute the variance and covariances.

Crescenti showed that these two methods produce similar results. He examined the effects of boxcar length on the fluxes and determined that a boxcar length of 6 km gave the best results. His results show that there are large, rapid changes in MABL temperature variances, heat and vapor fluxes in crossing the SST front. These changes are obtained by changes in the variances of the parameters with little change in correlation coefficients and phase angles. This suggests that turbulence increases intensity without change in eddy structure. A more thorough discussion is contained in Crescenti (1988, abstract attached in the Appendix).

From Crescenti's results it is obvious that the changes in turbulent statistics are strongest when the wind blows across the front from over the cold water to over the warm and least strong for the opposite wind direction. Crescenti and Stage (1992) uses the techniques developed by Crescenti (1988) to further study the behavior of atmospheric turbulence in the vicinity of the FASINEX front, especially the dependence on mean wind direction.

Herbster (1990) has used Crescenti's techniques to examine X-7 cross sections of the MABL fluxes. On Feb. 14 the wind was northerly in the FASINEX area and the Naval Research Laboratories (NRL) P3 aircraft flew a stack of 5 legs perpendicular to the SST and having elevations from 100 m to 1800 m. On Feb. 16 the wind was again northerly and the NCAR Electra and the flew the FASINEX flight box in formation. The result is two stacks perpendicular to the front with legs at 35, 100, and 945 m. Herbster's results support and expand on Crescenti's. The abrupt increases in heat flux, variance of vertical velocity, and variance of potential temperature at observed at low levels by Crescenti are seen to shift southward (downwind) and to become less abrupt at higher levels. Convective features that appear on all levels demonstrate the vertical continuity of these features. Given the two plus hours to complete each stack, Herbster's analysis also indicates that these features persist in time.

Friehe, *et al.* (1990, see abstract in appendix) draws together the work of several investigators to study the behavior of stress near the SST front.

3.2. Numerical Modeling.

The model used for this study was previously developed by Wai. This model consists of the Boussinesq primitive equations, second-order closure for turbulent fluxes, and a long wave radiative model. The model runs in an X-Z plane with the X axis perpendicular to the SST front. The front is assumed to be linear. The model has been modified to have open lateral boundary conditions so that it can be applied to the FASINEX situation. We know of no other such model. We have modified the model code to run on the Cyber 205 supercomputer at FSU and have improved the method used to solve the Poisson equation for pressure. Use of the supercomputer has enabled us to run the model for longer times and thus obtain better steady state solutions.

Results from the model have been reported in several conference papers (Stage, *et al.*, 1987a, b; Wai and Stage, 1987). In these papers we have concentrated on the structure of the MABL for geostrophic winds from the north, east, south, and west. These papers show how mean quantities of the MABL change across the front in each of these four cases and show that each wind direction produces a distinctive secondary circulation. A more detailed discussion of the behavior of the ABL for each of the test cases can be found in the abstracts and the articles.

One frustration in the modeling work has been that the strength of the secondary circulations seen in the model is generally about the same magnitude as the natural stochastic variability of the variables as seen in the data. This makes it difficult to make direct comparisons between the model results and the FASINEX observations, however some aspects of the model results do agree with the data.

4. Publications

4.1. Papers in refereed journals and Thesis.

Crescenti, G. H., 1988: Turbulent Variances and Covariances in the Marine Atmospheric Boundary Layer Over the FASINEX Front. M. S. Thesis, Florida State University, Tallahassee, Florida, 167 pp.

Crescenti, G. H., and S. A. Stage, 1992: Determination of Nonhomogeneous Turbulent Fluxes Near the FASINEX Sea Surface Temperature Front. Submitted to *Bound. Lay. Meteor.*

Friehe, C. A., W. J. Shaw, D. P. Rogers, K. L. Davidson, W. G. Large, S. A. Stage, G. H. Crescenti, S. J. S. Khalsa, G. K. Greenhut, and F. Li, 1990: Air-sea fluxes and surface-layer turbulence around a sea surface temperature front. *J. Geophys. Res.* **96**, C5, 8593-8610.

Herbster, C. G., 1990: The Vertical Structure of the Marine Atmospheric Boundary Layer Across a Sea Surface Temperature Front. M. S. Thesis, Florida State University, Tallahassee, Florida.

Wai, M. M. and S. A. Stage, 1989: Dynamical analyses of the marine atmospheric boundary layer near the Gulf-Stream oceanic front. *Quart. J. Roy. Meteor. Soc.*, **115**, 29-44.

4.2. Conference Papers

(In chronological order.)

Stage, S. A., M. M. Wai, and J. H. Crescenti, 1987: Atmospheric boundary layer structure near an oceanic SST front. Third Conference on Mesoscale Processes. August 21-26 1987. Vancouver, B.C. Canada, American Meteor. Soc., 206-207.

Stage, S. A., M.-K. Wai, and J. H. Crescenti, 1988: Atmospheric secondary flows in the vicinity of an oceanic front. Seventh Conference on Ocean-Atmosphere Interaction. February 1-5, 1988. Anaheim, California, American Meteor. Soc.

Stage, S. A., and R. A. Weller, 1985: The Frontal Air-Sea Interaction Experiment; Part I: Background and Scientific Objectives. *Bul. Amer. Meteor. Soc.*, **66**, 1511-1520.

Stage, S. A., and R. A. Weller, 1986: The Frontal Air-Sea Interaction Experiment; Part II: Experimental Plan. *Bul. Amer. Meteor. Soc.*, **67**, 16-20.

Wai, M. and S. A. Stage, 1988: A numerical study of the atmospheric boundary layer near an oceanic front. Eighth Symposium on Turbulence and Diffusion. April 25-29, 1988. San Diego, California, American Meteor. Soc. 309.

DTIC QUALITY INSPECTED 2

Accession For	
NTIS GRA&I	<input checked="" type="checkbox"/>
DTIC TAB	<input type="checkbox"/>
Unannounced	<input type="checkbox"/>
Justification	
By <u>Re: AD-A228140</u>	
Distribution/	
Availability Codes	
Dist	Avail and/or Special
<u>A-1</u>	

5. APPENDICES

This report includes the following appendices:

- 5.1 Abstract of G. H. Crescenti (1988).
- 5.2 Abstract of Mickey M-K Wai and Steven A. Stage (1989).
- 5.3 Abstract of Herbster (1990).
- 5.4 Abstract of Friehe, *et al.* (1990).
- 5.5 Manuscript of Crescenti and Stage (1992).

TURBULENT VARIANCES AND COVARIANCES IN THE MARINE
ATMOSPHERIC BOUNDARY LAYER OVER THE FASINEX FRONT

Gennaro H. Crescenti, M.S.
The Florida State University, 1988

Major Professor: Steven A. Stage, Ph.D.

A modified moving boxcar average and spectral filtering method are used to determine variances and covariances of meteorological variables in a nonhomogeneous marine atmospheric boundary layer (MABL). The data set analyzed was taken over the Sargasso Sea in the vicinity of an oceanic sea surface temperature front during the Frontal Air-Sea Interaction Experiment (FASINEX) in February 1986 by the NCAR Electra. The meteorological variables analyzed include the longitudinal, lateral and vertical velocities, potential temperature, and specific humidity in a three day case study in which an anticyclonic synoptic weather system north of the experiment area presented three different flow regimes.

The first day (16 February) is marked by a well mixed MABL with winds from the northeast across the front from cold to warm side. The second day (17 February) is also marked by a well mixed but deeper MABL with winds nearly parallel to the front from the east-southeast. The final day (18 February) shows increased atmospheric stability with a very shallow mixed layer with winds coming from the south-southeast across the front from warm to cold side.

Spectral analysis suggests the presence of a spectral gap in the frequency range of 0.0167 Hz or a period of approximately 60 seconds. This time scale is used as an averaging length for the boxcar method and as a cut off period for the spectral method. Each method shows good agreement with the other and displays the extent of the nonhomogeneity of the MABL.

The MABL across the oceanic front is found to be nonhomogeneous. The MABL parallel to the front is found also to be nonhomogeneous but to a lesser extent. Turbulent variances and covariances were found to be maximum when a component of the mean MABL wind blows across the front from the cold to warm side. The variances and covariances are less intense when the mean MABL winds are nearly parallel to the front and minimal when a component of the mean MABL winds blow from the warm to cold side.

5.2. Abstract of Mickey M-K Wai and Steven A. Stage (1989).

Dynamical Analyses of Marine Atmospheric Boundary Layer

Structure Near the Gulf Stream Oceanic Front

by

Mickey Man-Kui Wai and Steven A. Stage

Department of Meteorology

Florida State University

Tallahassee FL 32306

SUMMARY

The effects of the sea surface temperature (SST) front at the edge of the Gulf Stream on the marine atmospheric boundary layer (MABL) are investigated using a numerical model to study the modification effects of an oceanic front on the MABL structure. The situation simulated is flow from over cold shelf water to over the warm water of the Gulf Stream. The initial temperature and humidity profiles of the air are specified to be near neutral over the cold water and are therefore typical of undisturbed conditions. The differential in the SST across the oceanic front creates a horizontal variation in the surface perturbation pressure and the stability. The surface perturbation pressure and turbulent fluxes modulate the flow and produce horizontal variation in horizontal wind components with associated vertical motions. A thermally direct cell is produced as a result of the SST difference across the front. The isotherms slope upward towards the warm water. Entrainment of inversion layer air and upward vertical motion over the warm water cause the MABL to be deeper there. A layer of cloud forms over warm water and is associated with mixed layer deepening rather than lowering of the condensation level. Turbulent fluxes in the MABL show considerable spatial variation. Surface stress is much larger over the front and over the warm water than over the cold water. This is mostly caused by wind speed changes associated with the front. Changes in drag coefficient due to changes in surface roughness and stability are much less important.

Mean budgets for temperature and total water indicate that there is a balance between horizontal advection and turbulent flux divergence. The U momentum budget shows that once the geostrophic balance terms are subtracted off, the balance is mainly between the pressure gradient force associated with the induced temperature field and turbulent friction with horizontal advection and the Coriolis force acting on the geostrophic departure playing minor roles. The V momentum budget shows a balance between horizontal advection, Coriolis force and friction.

Although there is little data for comparison, the results are in qualitative agreement with observations in the area. This study shows that the SST front at the Gulf Stream edge produces marked local changes in the nearby atmospheric surface layer.

THE VERTICAL STRUCTURE OF
THE MARINE ATMOSPHERIC BOUNDARY LAYER
ACROSS A SEA SURFACE TEMPERATURE FRONT.

Christopher G. Herbster, M.S.
The Florida State University, 1990

Major Professor: Steven A. Stage, Ph.D.

The response of the lower marine atmospheric boundary layer to a sharp change in sea-surface temperature was studied in the Frontal Air-Sea Interaction Experiment (FASINEX) with ships and aircraft instrumented for turbulence measurements. The synoptic conditions on the 14th and 16th of February, 1986 presented the opportunity to study the vertical structure of the turbulence for the case of a North wind, blowing from the cold to warm side of the front. A moving boxcar averaging technique (after Crescenti, 1988) was used to determine the turbulent statistics and fluxes for the meteorological variables, and their associated changes, as the air made the transition from the cold to warm side of the front.

The data for this study were obtained from two aircraft, the NCAR Electra and NRL-P3, equipped for turbulence measurements in the atmosphere. The flight tracks for the two days were designed to investigate somewhat different aspects of the marine atmospheric boundary layer, concentrating on either the vertical structure alone (14 February) or on both the vertical and horizontal structure (16 February) in the vicinity of an oceanic temperature front.

The depth of the atmospheric boundary layer was found to be approximately 200 m deeper over the warm water than was found over the cold water. The potential temperature was found to respond very rapidly to the underlying warm water throughout the entire depth of the boundary layer. The increase in temperature was found to occur over a slightly broader region as the altitude was increased.

The vertical heat flux for each of the two days showed a pronounced increase over the warm water. While each day showed this general trend, there were distinct differences for the two days. The heat flux for the 14th showed two organized convective cells in the immediate vicinity of the front, one of which showed evidence of penetration into the inversion layer. This type of organized convection was not found on the 16th.

An analysis of the vertical momentum transfer, or stress, showed a nearly quadrature relationship between the horizontal and vertical velocity fluctuations. The phase relationship between these two variables was found to be more complicated than was found for the heat flux. Regions in the lower boundary layer in which the stress was found to be negative were found to coincide, in general, with regions which had about a 45° phase relationship between the two variables.

The variances of the meteorological variables were found, in general, to increase across the front over the warmer water. Both the vertical velocity and temperature fields showed a vertical structure which was in good agreement with previous boundary layer experiments. For both of these variables the maximum values for the variances were found to lie in the region between 30 and 60% of the depth of the boundary layer.

5.4. Abstract of Stage, *et al.* (1990).

Marine Atmospheric Boundary Layer Structure
in the Vicinity of a
Sea Surface Temperature Front

by

Steven A. Stage , William J. Shaw, Siri Jodha Khalsa,
Gary K. Greenhut, Gennaro H. Crescenti, Carl A. Friehe,
Catherine Gautier, Kenneth Davidson, Kristina Katsaros,
Mickey M-K Wai, David Rogers, Chris Herbster,
Richard Lind, and John Bates

Data from the Frontal Air-Sea Interaction Experiment (FASINEX) and results from boundary-layer models are used to examine the structure of the marine atmospheric boundary layer in the vicinity of a subtropical sea surface temperature (SST) front. Long and short wave satellite images are used to study cloud cover and radiative energy balances in the experimental region. Aircraft radiative and turbulence measurements are used to study changes in mean wind, temperature, humidity and mixed layer depth across the region of the SST front.

The wind direction relative to the SST front was different on each of the three flight days studied here. MABL structure is found to depend on whether the wind crossed the front from the cold to the warm side, was parallel to the front, or crossed it from warm to cold. The SST front was associated with substantial mesoscale features in the marine atmospheric boundary layer (MABL) flow on all three days. During cold-to-warm air flow the heat flux made a sharp transition at the front and a band of cloud was present just south of the front that appears to be connected to the front. A small pool of warm water at the northeast corner of the experimental area also produced substantial effects in the flux and cloud fields. For air flow nearly parallel to the SST front, There was a sharp north-south gradient in potential temperature near the front and little gradient away from the front. Details of the MABL structure near the front depend on small shifts in the relative alignment of the front and the wind. On the day with winds from warm-to-cold, a stable internal boundary layer grew near the surface and cut off turbulent mixing with the upper part of the MABL. Both daily and monthly radiation fields show modification by the SST front. Model computations give general agreement with the aircraft data and provide a helpful framework for interpreting boundary layer behavior.

5.5. Abstract of Friehe, *et al.* (1990).

Air-sea fluxes and surface-layer turbulence
around a sea surface temperature front.

by

C. A. Friehe, W. J. Shaw, D. P. Rogers, K. L. Davidson,
W. G. Large, S. A. Stage, G. H. Crescenti,
S. J. S. Khalsa, G. K. Greenhut, and F. Li

The response of the lower marine atmospheric boundary layer to sharp changes in sea surface temperature was studied in the Frontal Air-Sea Interaction Experiment (FASINEX) with aircraft and ships measuring mean and turbulence quantities, sea surface temperature and wave state. Changing synoptic weather on three successive days provided cases of wind direction both approximately parallel and perpendicular to a surface temperature front. For the wind perpendicular to the front, both wind over cold-to-warm and warm-to-cold surface temperatures occurred. For the cold-to-warm case, the unstable boundary layer was observed to thicken, with increased convective activity on the warm side. For the warm-to-cold case, the surface-layer buoyant stability changed from unstable to neutral or slightly stable, and the sea state and turbulence structure in the lower 100 m were immediately altered with a large decrease in stress and slowing of the wind. Measurements for this case with two aircraft in formation at 30 and 100 m show a slightly increased stress divergence on the cold side. The turbulent velocity variances changed anisotropically across the front: The stream-wise variance was practically unchanged, whereas the vertical and cross-stream variances decreased. Model results, consistent with the observations, suggest that an internal boundary layer forms at the sea surface temperature front. The ocean wave, swell and microwave radar back-scatter fields were measured from several aircraft which flew simultaneously with the low-level turbulence aircraft. Significant reductions in back-scatter and wave height were observed on the cold side of the front.

Determination of Nonhomogeneous Turbulent Fluxes Near the
FASINEX Sea Surface Temperature Front ¹

GENNARO H. CRESCENTI AND STEVEN A. STAGE

Department of Meteorology, Florida State University, Tallahassee, Florida 32306-3034.

^{*}This is FASINEX Contribution number 73.

ABSTRACT

Moving boxcar average and spectral filtering techniques are developed for use in determining position-dependent turbulent variances and covariances of meteorological variables in a nonhomogeneous marine atmospheric boundary layer (MABL). These techniques are used to analyze those variables observed in the vicinity of an oceanic sea surface temperature (SST) front over the Atlantic Ocean by the NCAR *Electra* during the Frontal Air-Sea Interaction Experiment (FASINEX). Measured variables include potential temperature, specific humidity, longitudinal, lateral and vertical wind velocity.

Spectral analysis suggests the presence of a spectral gap at wavelengths around 6 km. This scale is used as an averaging length for the boxcar and spectral methods. The two methods display the nonhomogeneity of the MABL and give good agreement for the magnitudes of the variances and covariances, and for the placement of features. The spectral method produces comparatively smooth curves while the boxcar method shows sharp jumps. We believe that these sharp jumps are real and indicate the edges of convective features of the MABL turbulence.

A three day case study is presented in which an anticyclonic synoptic weather system north of the experiment area presented three different MABL flow regimes. The first day is marked by a well mixed MABL with winds from the northeast blowing across the front from the cold to the warm side. The second day is also marked by a well mixed MABL with winds nearly parallel to the front from the east. The final day shows increased atmospheric stability with a very shallow mixed layer with winds from the south blowing across the front from the warm to the cold side.

Turbulent variances and covariances were found to be maximum when a component of the mean MABL blows across the front from cold to warm. The variances and covariances are less intense when the mean MABL winds are nearly parallel to the front and minimal when a component of the mean MABL winds blow from warm to cold side.

1. INTRODUCTION

Very little research has been conducted on the role of horizontal variability in air-sea interaction on spatial scales of less than several hundred kilometers and temporal scales of less than a day. Even less understood are the mechanisms by which horizontal variability on one side of the air-sea interface influences the fluid on the other side (Stage and Weller, 1985).

A cooperative, multi-investigator program was initiated to address this issue. The Frontal Air-Sea Interaction Experiment (FASINEX) (Stage and Weller, 1985; 1986) was a study of the response of the upper ocean to atmospheric forcing in the vicinity of an oceanic sea surface temperature (SST) front in the subtropical convergence zone southwest of Bermuda, the response of the lower atmosphere in that vicinity to the oceanic front, and the response of the associated two-way interaction between ocean and atmosphere. One of the major meteorological objectives of FASINEX was the determination of the mean and turbulent structure of the nonstationary, nonhomogeneous marine atmospheric boundary layer (MABL) in response to different sea surface forcing, synoptic scale forcing, and any existing or resulting induced secondary flow.

The mean and turbulent quantities in the MABL are not uniform across the oceanic front. Statistical methods used to characterize a horizontally homogeneous atmosphere may not adequately represent the MABL observed in FASINEX. Thus, this study was motivated to explore techniques in which to properly represent the various temporal and spatial scales that exist in a complex MABL.

Two techniques were examined and discussed (Crescenti, 1988) as methods for the determination of the turbulent variances of atmospheric variables (which describe the turbulent intensities) and the turbulent covariances (which describe the turbulent fluxes). The first method is a simple, unweighted moving average technique while the second is a spectral high pass / low pass, convolution technique. The atmospheric variables examined include the potential temperature, specific

humidity, longitudinal, lateral and vertical wind velocity. Both techniques were compared and were used to characterize the nonhomogeneous, nonstationary MABL for a three day case study in which the experiment area was under the influence of the same anticyclonic weather system but with three unique flow regimes with respect to the SST front.

2. NUMERICAL METHODS USED FOR FLUX COMPUTATION

2.1. *Description of the Problem*

The complexity of a turbulent flow is so formidable that even if we were able to describe its detailed structure, it would be impossible to comprehend (Businger, 1982). Consequently, the study of turbulence is directed towards describing its statistical characteristics.

The presence of a spectral gap allows us to separate the mean flow from the rapidly varying turbulent flow (Lumley and Panofsky, 1964; Fielder and Panofsky, 1970; Panofsky and Dutton, 1984). A realization $f(t)$, which is a function of time t can be represented as

$$f(t) = \bar{f} + f'(t) \quad (1)$$

where \bar{f} is the mean, defined over some interval T as

$$\bar{f} = \frac{1}{T} \int_{-T/2}^{+T/2} f(t) dt \quad (2)$$

and $f'(t)$ is the fluctuation about the mean. This separation of scales is known as Reynolds decomposition (Tennekes and Lumley, 1972) where the mean is usually treated as a deterministic quantity (Panofsky and Dutton, 1984) and the statistical behavior of $f'(t)$ is analyzed.

Randomness is unavoidable. It is an intrinsic property of all turbulent flows (Tennekes and Lumley, 1972) and is related to the fact that the details of a flow are not repeatable. The problem is

complicated when nonstationary processes are added to a turbulent flow. In FASINEX, the synoptic scale forcing of the MABL was not constant during the time required for an aircraft to traverse its flight path, which was on the order of only several hours. Even greater complexity is added to the problem when spatial variability is superimposed to the flow. In the case of FASINEX, the MABL was forced by a sharp, step-like sea surface temperature front. Thus randomness, temporal variation and spatial variation are all intermingled in the data and are not easily separated. The very nature of a complex, nonstationary, nonhomogenous MABL prevents a single, clean-cut partitioning of mean and turbulent parts.

Ordinarily, when using the traditional eddy correlation method, the variance of a variable f is

$$VAR_f = \frac{1}{T} \int_{-T/2}^{+T/2} (f(t) - \bar{f})^2 dt \quad (3)$$

and the covariance between two variables f and g is

$$COV_{fg} = \frac{1}{T} \int_{-T/2}^{+T/2} (f(t) - \bar{f}) (g(t) - \bar{g}) dt. \quad (4)$$

Usually, a time series record is arbitrarily broken up into intervals or blocks of fixed length or duration. Within each block, a single mean and variance are computed. It is common to use a linear least-squares fit to remove time trends from the data within each interval before computing the variance and/or covariance. This method of computing statistics in the complex MABL found in FASINEX may not be entirely satisfactory.

An aircraft traveling at 100 m s^{-1} covering a path length of 36 km is roughly equivalent to the field length that blows past a fixed instrument over a one hour period at 10 m s^{-1} . The aircraft would be able to transit the 36 km in just 6 minutes, thereby minimizing the effects of

nonstationarity. This also cuts down on the amount of averaging time by approximately an order of magnitude (Wyngaard, 1973).

The spectral gap for fixed point data in the atmospheric boundary layer usually has a period of 30 minutes to 2 hours. Analysis of the FASINEX data (Crescenti, 1988) suggest a spectral gap of approximately 1 minute which corresponds to a path length of approximately 6 km for an aircraft traveling at 100 m s^{-1} . Qualitatively, this is in good agreement with theory.

2.2. Boxcar Method

This first method which we develop for computing turbulent variances and covariances is based on simple, unweighted, moving averages (see e.g. Holloway, 1958). A boxcar average is computed by integrating over a time interval of length T centered at time t and then dividing by T . All of the filter weights for the boxcar are equal to $1/T$.

Let the boxcar average of any random time series $f(t)$ be defined by

$$\bar{f}(t) = \frac{1}{T} \int_{-T/2}^{+T/2} f(t+t') dt', \quad (5)$$

where t is the time, t' is dummy variable for integration over the boxcar, and T is the time length of the boxcar. The covariance of $f(t)$ and $g(t)$ is defined by

$$\begin{aligned} \text{COV}^*(f, g)(t) = \frac{1}{T} \int_{-T/2}^{+T/2} & (f(t+t') - \bar{f}(t)) \\ & (g(t+t') - \bar{g}(t)) dt'. \end{aligned} \quad (6)$$

The boxcar variance of any variable, f , is simply defined as the covariance of that variable with

itself, namely:

$$VAR^*(f)(t) = COV^*(f, f)(t). \quad (7)$$

The correlation between two variables is given by

$$COR^*(f, g)(t) = \frac{COV^*(f, g)(t)}{[VAR^*(f)(t) VAR^*(g)(t)]^{1/2}}. \quad (8)$$

The asterisk superscript indicates that the variables are not detrended. It should be emphasized that the mean, covariance, and correlation are all functions of time. Note also that these statistics can not be computed within $T/2$ of either end of a time series. We have emphasized the time dependence COV and VAR by explicitly writing it in the equations above. For convenience, we will now omit showing this time dependence.

Linear trends in \bar{f} and \bar{g} will contribute to $COV^*(f, g)$. We generally do not want to include this as turbulent covariance. We therefore detrend the data in a way which is similar to that commonly used when the data is broken into blocks. The simplest computational method for this is to let the detrended covariance between f and g be given by

$$COV(f, g) = COV^*(f, g) \left[1 - \frac{COR^*(f, t) COR^*(g, t)}{COR^*(f, g)} \right], \quad (9)$$

where $COR^*(f, t)$ is the correlation between f and time, and $COR^*(g, t)$ is the correlation between g and time. It can be shown that linear trend in f or g does not contribute to $COV(f, g)$ defined in this way and, therefore, that the effects of linear trends have been removed.

When the mean of f has a change which is rapid and is not linear within a boxcar, this will contribute to $VAR(f)$, however $VAR(f)$ is much less sensitive to such contamination than $VAR^*(f)$. This makes detrended statistics superior to non-detrended statistics for separating the mean and turbulent components of the flow. A specific example occurs in potential temperature on

17 February. Mean θ changes steeply near the SST front. This produces a large peak in $VAR^*(\theta)$, but much less of a peak in $VAR(\theta)$.

Detrended variance and correlation (VAR and COR) can be defined in an obvious way by using detrended (unstarred) statistics in (7) and (8).

The statistics defined by (5) through (9) have been chosen for some important properties. Note that $\bar{f}(t)$ and $\bar{g}(t)$ on the right hand side of (6) are functions of t rather than $t+t'$. This is a different result than would be obtained by first using a high pass boxcar filter on f and g to get f' and g' , then using a low pass boxcar filter on the product $f'g'$. That statistic would correspond to use of

$$COV^*(f, g)(t) = \frac{1}{T} \int_{-T/2}^{+T/2} (f(t+t') - \bar{f}(t+t')) (g(t+t') - \bar{g}(t+t')) dt'. \quad (10)$$

There are some important advantages of using (6) instead of (10). First, it can also be shown that when (5), (6) and (9) are used to evaluate $COV(f, g)(t)$ at $t = t_k$ the result is the same as taking the data within the interval I_k , detrending it then using (2) and (3) to compute $COV(f, g)_k$. This states that the boxcar statistics, as defined here, give the exact same values as the interval statistics for those time points where interval statistics can be computed. Because of this important property, values obtained by the boxcar method can be compared with those from many previous studies. Second, means and covariances found from (5)–(9) obey the Reynolds postulates (e.g., Lumley and Panofsky, 1964; Panofsky and Dutton, 1984; Stull, 1988). The Reynolds postulates are:

$$\bar{f}' = 0, \quad (11)$$

$$COV(\bar{f}, f') = 0, \quad (12)$$

and

$$\overline{\overline{f}} = \overline{f} \quad (13)$$

Covariances computed using (10) are differentiable and continuous but do not satisfy (11)–(13) (Panofsky and Dutton, 1984). Thus values computed using (10) do not satisfy the equations of motion as they are commonly derived for turbulence work, while those computed using (5)–(9) do. In practice this advantage from the use of (5)–(9) instead of (10) is mostly conceptual. If the boxcar length corresponds to a period which is within a well-defined spectral gap, then statistics found by using (10) nearly satisfy (11)–(13) and therefore nearly satisfy the equations of motion.

2.3. *Spectral Filter Method*

The second method involves the application of high and low pass filters. An analogous representation of Reynold's decomposition using spectral filtering may be thought of as

$$f(t) = LP\{f(t)\} + HP\{f(t)\}, \quad (14)$$

where $LP\{f(t)\}$ represents the low pass filter or mean of $f(t)$ and $HP\{f(t)\}$ is the high pass filter or perturbation of $f(t)$. The high pass filter used here takes the fast Fourier transform (FFT) of $f(t)$, sets all frequencies lower than a specified cut off frequency to zero, and then takes the inverse FFT. Similarly, the low pass filter sets all frequencies greater than the cut off frequency to zero.

Using these filters, we can then compute the covariance of two random time series by multiplying the high pass filtered results of $f(t)$ and $g(t)$ and then applying a low pass filter to that product. This can be represented as

$$COV(f, g) = LP\{HP\{f(t)\} HP\{g(t)\}\} \quad (15)$$

The spectral method can also be used to obtain information about the phase relationship between $f(t)$ and $g(t)$. We can compute the quadrature covariance much like the covariance in the steps given above except that a Hilbert transform, $H\{\}$, is applied to $g(t)$, thus the quadrature covariance is

$$QCOV(f, g) = COV(f, H\{g\}), \quad (16)$$

and the quadrature correlation is defined as

$$QCOR(f, g) = COR(f, H\{g\}). \quad (17)$$

The coherence and the phase angle between $f(t)$ and $g(t)$ are then, respectively,

$$COH(f, g) = [COR(f, g)^2 + QCOR(f, g)^2]^{1/2}, \quad (18)$$

and

$$PHASE(f, g) = \arctan \left[\frac{QCOR(f, g)}{COR(f, g)} \right]. \quad (19)$$

The definitions (16)–(19) are based on several properties of the Hilbert transform (Bendat and Piersol, 1986). First, the Hilbert transform accomplishes a $-\pi/2$ rotation in phase space, i.e., $H\{\sin(\omega t)\} = \sin(\omega t - \pi/2)$ and $H\{\cos(\omega t)\} = \cos(\omega t - \pi/2)$. Secondly, the Hilbert transform of a signal is orthogonal to that signal, i.e.,

$$\int f(t) H\{f(t)\} dt = 0, \quad (20)$$

where the integral is taken over the entire flight leg. We interpret $COR(f, g)$ to be a measure of how closely variations in f and g are connected to each other; $COR = 0$ represents no connection and $COR \approx \pm 1$ represents strong connection. However, two signals which vary $\pi/2$ out of phase with each other have $COR = 0$ even though there is a strong connection between them. $QCOR$

is a measure of such a connection at $\pi/2$ phase difference. *COH* combines the in-phase and the quadrature correlations to tell how tightly f and g are connected at arbitrary phase. If we let f_ϕ be the time series obtained by shifting f by an angle ϕ in phase space and compute $COR(f_\phi, g)$, then $COH(f, g)$ is the maximum value which can be obtained for $COR(f_\phi, g)$, and $PHASE(f, g)$ is the value of ϕ which produces that maximum.

Like the boxcar technique, the spectral technique produces variances and covariances which satisfy (11)–(13) exactly, and therefore, can be used in the equations of motion as they are classically obtained by Reynold's decomposition.

The spectral method assumes periodicity in a realization. As a result a trend in the data can produce an apparent discontinuity between the ends of the flight leg that can contaminate the data near either end. Linear detrending of the entire flight leg before taking the FFT reduces the size of the discontinuities introduced but does not entirely remove this contamination. It is interesting to note that the contamination in variances and covariances computed by the spectral method occurs in regions of order $T/2$ long at either end of the time series. Thus, the spectral method is unreliable in the same regions where the boxcar method can not produce values. This is a fundamental property of these techniques which is caused by the fact that both require data from about $T/2$ on either side of the computation point.

The FFT filter has the sharpest possible cut off in the frequency domain. This corresponds to the very gradual $\sin(ft)/ft$ window in the time domain. The boxcar filter represents the opposite extreme. It has the sharpest possible cut off in the time domain and has a very gradual $\sin(ft)/ft$ window in the frequency domain. It is possible to define any number of covariances similar to (15) simply by using different high and low pass filters. It is also possible to use non-uniform weights in the boxcar averaging done by (5)–(9). In fact, any weighted boxcar filter can be expressed in the form of a spectral filter, (15); and any spectral filter can be expressed as a weighted boxcar

filter. All other filters which one might be tempted to use lie between these two extremes. Since these two methods utilize different approaches in determining the same statistic, it is useful to look at the results of both methods. Any qualitative or quantitative behavior which is seen by both methods can be considered present in the data rather than being an artifact of the computational method used. By comparing results from these two methods, we gain confidence that features seen in results of both methods would also appear in output from any reasonable averaging method. Friehe *et al.* (1990) have compared the fluxes obtained using this boxcar method and this spectral method with those obtained using (15) and have found that all give good qualitative agreement for the major features seen in the surface stress across the FASINEX SST front.

3. DATA AND METEOROLOGY

Data presented in this study were acquired by the NCAR *Electra* and include the sea surface temperature, potential air temperature, specific humidity, and longitudinal, lateral and vertical wind velocity. The SST was acquired at 1 Hz, whereas the rest of the variables were sampled at 20 Hz.

Post experiment data processing was carried out at the NCAR Research Aviation Facility (Miller and Friesen, 1985). The data obtained by the *Electra* were excellent in overall quality with minimal data loss (Griffith, 1986). Additional processing (Crescenti, 1988) included correction of data spikes due to radio interference, radiometric surface temperature correction (Liu and Katsaros, 1984), correction of the Schuler oscillation in the horizontal wind velocity (Shaw, 1988), and specific humidity computation from a Lyman-alpha hygrometer (Schanot, 1987).

An interleaved box flight pattern was designed to examine cross frontal features in the MABL (Figure 1). Information received from satellite and ship reports prior to each flight was used to center the box on a portion of the SST front which ran in a nearly linear east-west fashion. The

Fig. 1

box contained four north-south oriented (cross-frontal) legs which were 100 km long and spaced 30 km apart. These legs are labeled as 7-8, 2-3, 5-6 and 4-1, respectively from west to east. A redundancy factor was intentionally built into the flight box for the purpose of examining time trends in the meteorological data. This is accomplished by comparison of several overlapping east-west legs. The *Electra* flew approximately 35 m above the sea surface at 100 m s^{-1} . About 2 to 2.5 hours were required to complete the flight box.

FASINEX was under the influence of an anticyclonic system that moved across the Atlantic Ocean north of the experiment area over the course of three days. The start of the period was marked by the rapid passage of cold front through the experiment site at 00 UTC on 16 February. The translation speed of the cold front was estimated at 70 km hr^{-1} relative to the positions of the R/V *Oceanus* and R/V *Endeavor* (Mundy, 1987). By the time the *Electra* was on station (15 UTC), the high pressure system became the dominant synoptic weather feature. Mean wind speeds averaged 8 to 9 m s^{-1} from the northeast during the *Electra* flight. By 00 UTC on 17 February, the high pressure moved further east to 33°N , 68°W , just west of Bermuda. The wind was from the east at 8 to 10 m s^{-1} during the second *Electra* flight. On 18 February, the anticyclone continued its eastward progression and was centered at 33°N , 60°W , just east of Bermuda. Winds were observed on the *Electra* from the south-southeast at 8 to 10 m s^{-1} .

This sequence of weather events was quite fortuitous for FASINEX. One of the principle goals of the project was to examine the horizontal variability due to different scales of synoptic forcing. In this case, the experiment area was under the influence of the same anticyclonic system but under three unique flow regimes relative to the SST front. The wind blew across the front from the cold to the warm side on the first day, was nearly parallel to the front on the second day, and blew across the front from the warm to the cold side on the final day.

4. COMPARISON OF BOXCAR AND SPECTRAL METHODS

The variances and covariances determined by the boxcar and spectral methods are in very good quantitative and qualitative agreement with each other. Both give time varying fluxes and show rapid changes near the front.

A series of plots of potential temperature variance are shown using various boxcar averaging lengths (Figure 2) and spectral cut off frequencies (Figure 3). This example enables us to examine the behavior of both computational methods and how they represent the turbulence using various time averaging scales. The averaging times for the boxcar method in this series are 15, 30, 45, 60, 120, 180, 240, and 360 seconds. This corresponds to averaging lengths ranging from 1.5 to 36 km. The same analogous frequencies are used for the spectral filter series. A cross frontal leg was selected to point out the features of each method and how they represent sudden changes in the turbulence in the MABL across the front.

Fig. 2Fig. 3

As expected, the boxcar and spectral methods display considerable variability at very small averaging times or at very high cut off frequencies, respectively. As we move towards longer averaging times or lower cut off frequencies, much of the variability is reduced and large scale features become more readily apparent. At a 60 second averaging time with the boxcar method, a sudden increase in the temperature variance is observed over the warmer water. This is also observed with the spectral method with the same analogous cut off frequency, however, the change in the temperature variance is not as abrupt or as well defined. As we continue on to longer averaging times or lower cut off frequencies, much of the detail is lost to smoothing. Also note for the boxcar method, a significant amount of information is lost at either end of the flight leg. The sudden change in the variance at the SST front becomes less obvious with both methods.

Basically, we are faced with a compromise. Too short an averaging time preserves sharpness of features, but leaves too much randomness in the results. Too long an averaging time removes

the randomness, but also sacrifices sharpness of features by smearing them horizontally. This is analogous to the averaging time problem faced by Lumley and Panofsky (1964) who conclude that the smallest uncertainties in the turbulent variances and covariances are obtained when the division between deterministic and turbulent parts of the flow is made using an averaging time which lies in a spectral gap. An averaging time of 60 seconds is supported by spectral analysis of the data (Crescenti, 1988). For most legs, temperature and vertical velocity show that 6 km is in the spectral gap or at least on a shoulder of the spectrum. Averaging time also agrees with results found by Friehe *et al.* (1990) by use of ogive analysis of cospectra.

The boxcar technique often shows changes at the SST front which are much more abrupt than those shown by the spectral method. The boxcar technique does not artificially impose any sharp-edged features on the flow. Sharp edged features nonetheless appear in the boxcar statistics. These correspond to sharp changes in the variance of the data which can be seen in the original 20 s^{-1} time series. For instance on 16 February θ shows a sudden increase in variance over the SST front which is conspicuous in the 20 s^{-1} time series. Boxcar $VAR(\theta)$ (Figure 7) shows a similar sudden change. Spectral $VAR(\theta)$ shows a more rounded increase. We therefore favor the boxcar results as being more consistent with what our eyes see in the time trace. We thus emphasize the boxcar results in this paper.

Conditional sampling analysis is based on observations of such sharp features in time traces and uses on/off indicator functions to represent these sharp edges. The sharp edges seen in the boxcar technique thus lend support to conditional sampling analysis.

The boxcar technique takes the initial time series $f(t)$ and produces time series $\bar{f}(t)$ and $COV(f,g)(t)$ each of which have the same number of points per second as the original (although the $\bar{f}(t)$ time series is shorter by a time T). However, The number of degrees of freedom are greatly reduced. The original time series has a number of independent data points which depends on the

integral time scale of the flow (Tennekes and Lumley, 1972). There is only one independent data point in $\bar{f}(t)$ and $COV(f,g)(t)$ for each boxcar. (Choice of the boxcar length in the spectral gap means that the integral time scale of the flow must be less than the boxcar length.)

The boxcar technique also provides some insight into the error bars associated with the traditional method of computing fluxes. Even stationary data will show a certain amount of stochastic variability in $COV(f,g)(t)$. For a stationary time series, the standard deviation of $COV(f,g)(t)$ within any interval I_k is equivalent to the standard deviations of the values which might be obtained for $COV_k(f,g)$. This can readily be seen by considering the fact that when we divide the data into intervals, we choose the time used for $t = 0$ in a completely arbitrary manner. In this context, one advantage of the boxcar method is that it allows us to look at all of the answers we could have gotten from the block mean method if only we had started our clock at a different time.

For nonstationary data, features within the flow are able to choose their own boundaries when they are analyzed by the boxcar method rather than having positions imposed on them by the choice of $t = 0$ as would be done with the block mean method.

We will now turn our attention to analyzing the turbulent variances and covariances using a 60 second boxcar average.

5. CASE STUDY — THREE DIFFERENT FLOW REGIMES

5.1. 16 February 1986

This day is marked by a shallow but well mixed MABL with winds blowing from the northeast across the SST front from cold to warm waters. A three dimensional representation of the SST pattern is shown in Figure 4. The SST front is quite distinct on this day and runs in an east-west fashion slightly north of the middle in the FASINEX box. Temperature jumps are approximately 2 C over distances of 2 to 10 km. The boxcar mean of the potential temperature shows the influence

Fig. 4

of the sea surface temperature pattern (Figure 5). The potential temperature increases by about 1 °C from the northern end to the southern end of the 100 km flight legs. For each of the four legs, the steepest rate of change is located about 20 to 40 km south of the front. The boxcar average of the specific humidity shows a different behavior (Figure 6). The values of humidity range from 6.5 to 8.5 g kg⁻¹. Dry zones appear in three of the four legs at and just to the north of the SST front. These plots also show that the specific humidity increases at the north-most ends of legs 4-1 and 5-6 over a pool of warm SST. This warm pool seems to be the most likely cause of these high specific humidities, although, it is also possible that a subsidence region over the front contributes to the relatively dry region seen 0 to 20 km north of the front on legs 4-1 and 5-6.

The potential temperature boxcar variance shows a dramatic increase in turbulence in the vicinity of and to the south of the SST front in all four legs (Figure 7). This turbulent intensity is maintained for approximately 30 to 40 km south of the front. The same is observed for the vertical velocity variance (Figure 8). South of the front, specific humidity variance (Figure 9) increases somewhat but the change is much less dramatic than for the other two variances. This is due to the fact that the humidity difference between the air and the sea surface does not change as much at the front as the air-sea temperature difference.

The turbulent fluxes respond very quickly to the large air-sea temperature differences induced by the warm water and give maximal fluxes just south of the front. As the air moves southward, it is warmed and moistened. The air-sea temperature and humidity differences become smaller and the MABL becomes less unstable. This leads to a reduction in fluxes toward the southern ends of the legs. This analysis is in agreement with that found in Friehe *et al.* (1990).

The kinematic vertical heat flux (Figure 10) greatly increases just south of the SST front. Also note that smaller strong convective cells are present in this unstable region, showing that the turbulence is concentrated in smaller pockets approximately 5 to 10 km wide rather than being

uniformly distributed throughout the region.

This paper mostly concentrates on using the boxcar method to show spatial variations associated with the SST front. Here we see that the boxcar method also provides a tool for portraying and quantifying the spatial variations in turbulent structure which are associated with small mesoscale features that are present in the MABL but that do not owe their existence to the front and that have positions with no fixed relationship to the front.

The kinematic moisture flux (Figure 11) is similar to the heat flux, however, the transition at the frontal region is not as dramatic. A strong upward transport of water vapor is observed for about 20 *km* south of the front in leg 2-3. Smaller isolated pockets of upward moisture flux are observed in the other legs. Again, the large positive flux regions are strongly correlated with values similar to that of the heat flux.

Fig. 11

The kinematic momentum flux (Figure 12) is negative at all locations. This shows the downward transport of momentum from higher levels of the MABL to the surface. The largest downward flux occurs about 20 *km* south of the front on leg 2-3 which is coincident with the large upward transport of heat and moisture noted above. This reinforces our conviction that this is a region of strong mechanical and thermal mixing.

Fig. 12

The coherence between vertical velocity and potential temperature (Figure 13) is quite high, hovering around 0.6 over the warm water and ranging from 0.5 to 0.6 over the cold water. There are no sharp changes in coherence to correspond with the sharp changes seen in covariance at the front. We thus see that as the air crosses the front, the turbulence responds by increasing the variances of vertical velocity and potential temperature, but that there is only a very slight increase in the efficiency of heat transport as measured by the coherence. This can be interpreted as an indication that the amplitude of turbulence increases without much change in turbulent structure, at least not in any way which effects the coherence. The active mixing region near 20 *km* south of the front

Fig. 13

on leg 2-3 is not visible in the coherence. Evidently the MABL over the cold water was sufficiently unstable to organize the turbulent convection about as much as possible and to give near maximal values of coherence. The greater instability south of the front was not able to much further organize convection. Nor was the active convection region on leg 2-3 any more organized.

Coherence between vertical velocity and specific humidity (not shown) was mostly between 0.4 and 0.6 with average about 0.5. No pattern associated with the front is visible. There are, however, two peaks of coherence (value 0.6) that correspond to the two peaks in covariance on leg 2-3. Examination of the convective region on leg 2-3 shows that variances of vertical velocity and potential temperature are large there, but that variance of specific humidity is small there. The peak in moisture flux (covariance) is then accomplished by increased mixing (variance of vertical velocity) and by increased efficiency (coherence) at vapor transport, but actually shows a decrease in humidity variance.

Phase angle between vertical velocity and potential temperature (not shown) is mostly between -10 and 5 degrees with average about -5 degrees. Phase angle between vertical velocity and specific humidity (not shown) is mostly between -20 and 20 degrees with average near 0. This indicates that there is little quadrature relationship between these pairs of variables and is one distinguishing feature between turbulent flow and flows containing waves.

The coherence between vertical and horizontal velocity has an average of about 0.25 and is much weaker than the previously mentioned coherences. These two variables were found to be approximately 150 degrees out of phase.

This day exhibits MABL characteristics associated with air modification due to advection of (relatively) cold air across the SST front. The results of this study show how very rapidly the MABL turbulence is changed by the sudden instability induced by the change in surface conditions.

5.2. 17 February 1986

This second day is also marked by a well mixed but deeper MABL. Winds on this day are from the east which are nearly parallel to the SST front. The MABL was both warmer and more moist than on the previous day. The formation of a shallow internal boundary layer (IBL) is observed over the cold water (Rogers, 1989). A three dimensional plot of the SST is shown in Figure 14 . Fig. 14

The potential temperature (Figure 15) changes about 1 C over the 100 km span. On this day, Fig. 15

the temperature is fairly isothermal on either side away from the front. Legs 4-1, 5-6, and 7-8 have steep, narrow regions near the front in which potential temperature changes. Leg 2-3 has a region of moderate temperatures 0 - 40 km south of the front. The specific humidity (Figure 16) is higher on this day and is fairly constant with values ranging from 9 - 10 g kg⁻¹. The small Fig. 16

air-sea temperature and humidity differences on this day produce much smaller fluxes and variances compared with the first day and give much less turbulent mixing in the MABL.

As on the 16th, the potential temperature variance (Figure 17) and the vertical velocity Fig. 17

variance (Figure 18) are much larger over the warm water than over the cold. However, these Fig. 18

variances change in a much wider region than on the 16th. Specific humidity variance (Figure 19) has no apparent changes at the front. More turbulent convective mixing is evident south of the Fig. 19

SST front whereas much of the mixing is limited to within the shallow IBL in the north (Rogers, 1989).

The magnitude of the kinematic heat flux is nearly zero over the colder water indicating near neutral conditions (Figure 20). However, the flux becomes positive on the warm side of the front Fig. 20

indicating an upward transport of sensible heat. However, the absolute magnitude of the flux is much less than observed on the first day. The transition region is very sharp and is located right at the SST front. This indicates a very different picture of the response of the turbulence to the front than on the 16th. On this day the sharp change in heat flux at the front is the result of a sharp

change in correlation (Figure 21) between vertical velocity and potential temperature. On this day the air over the cold water is near neutral and has little organization for heat flux. Correlation averages about 0.2. Immediately south of the front, the turbulence becomes more organized for heat flux and the correlation takes a sharp jump to about 0.4. This produces a sharp jump in heat flux even though the vertical velocity and potential temperature fluctuations change over a much broader region.

Fig. 21

The kinematic moisture flux (Figure 22) resembles the heat flux. It has positive values throughout the entire leg with the largest values south of the front. There is a sharp transition near the front, which is caused by a sharp change in correlation between vertical velocity and specific humidity. Specific humidity variance (Figure 19) shows no discernible changes at the front. The kinematic momentum flux is only slightly larger south of the SST than to the north (Figure 23). Again, this indicates more mixing of the MABL south of the front. The two variables are fairly correlated with a typical value of 0.4.

Fig. 22

Fig. 23

On this day the MABL can be viewed as two side-by-side mixed layers; one over the warm water and one over the cold (Stage, *et al.*, 1990). There is little advection between these two MABL's and as a first approximation they can be viewed as separate and having turbulent properties appropriate for their own local conditions.

5.3. 18 February 1986

This final day is marked by an increase of atmospheric stability with winds blowing from the south across the front from the warm to the cold water. These winds bring air into the FASINEX area that is warmer and more moist than either of the other two study days. Again, a shallow IBL is observed over the cold water (Rogers, 1989). This gives a decoupling of the MABL from the cold water surface, and the MABL is not well-mixed north of the front. As a result, quantities

measured at the flight level are less representative of the surface than on the previous two days. The SST frontal gradients (Figure 24) have decreased on this day. The mean potential temperature (Figure 25) is nearly isothermal south of the front, but decreases in a nearly linear fashion after crossing the frontal region to the north. The total drop in temperature is only about 0.6 to 0.8 C. Data from leg 7-8 are cut short because of rain squalls encountered on the west side of the FASINEX box. The mean specific humidity values (Figure 26) increased on this final day to about 12 to 13 $g\ kg^{-1}$. Legs 2-3 and 5-6 show a dry zone region in the vicinity of the SST front. This dry zone is most likely the result of subsidence over the front.

The magnitudes of the potential temperature variance (Figure 27) are the smallest on this day. The values over the cold water are somewhat larger than over the warm water. Note the region of large variance seen in leg 5-6 about 5 to 15 km north of the front. This is not a real feature of the MABL. Rather, it is an artifact of variance created by the boxcar technique. In this region the mean potential temperature has nonlinear changes with spatial scales shorter than the boxcar length. The boxcar technique inappropriately interprets these as turbulent variance. Essentially this is a inherent limitation in the ability of the boxcar method to partition the flow into mean and turbulent components. Turbulent mixing is still evident south of the front in the vertical velocity variance (Figure 28). The vertical humidity variance (Figure 29) is similar to the potential temperature variance. North of the front in the more stable region, the vertical velocity variance is near zero.

The vertical velocity variance (Figure 28) has behavior opposite to the potential temperature variance with largest values over the warm water. The kinematic heat flux (Figure 30) is slightly positive south of the SST front but actually reverses its sign north of the front where there is a downward flux of sensible heat. The reversal from slightly unstable to stable takes place exactly over the front.

The kinematic moisture flux (Figure 31) is positive south of the front. At most locations north of the front it is near zero due to the decoupling of the flight level from the surface. South of the front, the humidity flux shows pseudo-periodic oscillations that have wavelength of about 10 km. These may indicate the presence of horizontal roll vortices, but further study would be needed to confirm this conjecture.

Fig. 31

Figure 32 shows that the magnitude of the kinematic momentum flux is much less north of the front than south of it. Leg 5-6 has the most dramatic drop, changing from an average of about $-0.1 \text{ m}^2 \text{ s}^{-2}$ to about $-0.05 \text{ m}^2 \text{ s}^{-2}$ in less than 10 km right at the front. Leg 2-3 also has a sudden change, while leg 4-1 is much more gradual.

Fig. 32

On this day the correlation between vertical velocity and potential temperature (Figure 33) is 0.3 to 0.4 south of the front and around -0.4 north of the front. These two regions are joined by a broad nearly linear region from about 20 km south of the front to 10 km north of it. Perhaps the most remarkable feature of this transition is that it begins some 20 km upwind of the front thus indicating that the turbulence can somehow anticipate the surface changes at the front. The most likely explanation of this fact is that secondary circulations are induced in the MABL and that the associated pressure gradients and vertical motions influence the turbulence upwind of the front.

Fig. 33

The changes in vertical velocity variance at the front are moderately abrupt while changes in potential temperature variance and kinematic heat flux are much more gradual. This slow transition in heat flux is unique among the three study days and indicates that this unstable-to-stable transition is much more gradual than the stable-to-unstable transition seen on 16 February. The frontal changes seen on 17 February are made sharp by the smallness of the advection across the front that gives the air long times to adjust to the new surface conditions. On 18 February the transition is made gradual, as the stable IBL chokes off mixing.

6. SUMMARY AND CONCLUSIONS

FASINEX was the first ambitious attempt to study horizontal variability of air-sea interaction. The major objective of this study is the determination and behavior of turbulent variances and covariances in a nonhomogeneous MABL in response to different sea surface and synoptic scale forcing.

The results shown here demonstrate that the boxcar and spectral filter techniques yield an understanding of spatially varying turbulent statistics. Both techniques show promise for revealing the nature of the turbulent MABL in nonhomogeneous situations. However, the simple boxcar method depicts the turbulence in a more detailed manner, whereas the spectral method tends to represent the turbulence in a smoother, sinusoidal flow.

We have used the boxcar method to examine the behavior the variances and covariances from data for three consecutive days having different wind directions. On the first day the wind blew across the front from the cold to warm water, blew nearly parallel to the front on the second day, and then blew across the front from warm to cold water on the last day. A 60 second averaging time corresponding to a 6 km length average was used to determine the turbulent statistics.

The MABL is found to be nonhomogeneous across a SST front. When the winds are found to blow across the front from cold to warm water, the MABL has the most intense turbulence and largest fluxes. These largest of these fluxes are found just south of the SST and extend for about 30 km. The turbulent variances and covariances are less intense when the winds are found to be nearly parallel to the SST front. Finally, when the winds blow across the front from warm to cold water, the MABL is found to be nearly neutral to slightly stable, for the two sides of the front respectively. The largest of fluxes were still found south of the front but reduced to zero or switched signs north of the front. The turbulence on each of the three case study days demonstrates distinctive behavior which is related to the changes in stability and to the advection times.

There are some differences between the individual flight legs on any given day. These are associated with organized mesoscale convective regions. However, for the most part, major features associated with the front have behavior which is the same for all legs of each day.

Acknowledgments.

Most of this work was done at Florida State University as part of the first author's Master's thesis and was supported by a grant from the Marine Meteorology Program of the U.S. Office of Naval Research. Portions of this manuscript were prepared while the first author was employed at Woods Hole Oceanographic Institution.

The authors wish to thank the U.S. Office of Naval Research for their role as primary sponsors of FASINEX as well as the other sponsoring agencies for their participation. We are also indebted to the other scientists and numerous support personnel who participated in FASINEX. Special thanks go out to Christopher Herbster for his help with much of the programming and plotting of the data and to Carl Friehe, Robert Weller and Richard Payne for their encouragement and comments during the preparation of this manuscript.

Many thanks to the flight crew of the NCAR *Electra* who flew us around in countless circles during FASINEX without once complaining. Thanks also to the NCAR Research Aviation Facility for their help with some of the post experiment data correction.

7. TABLE OF FIGURES

Fig. 1. The FASINEX flight box. The box was flown from in the order 1, 2, 3, 4, 1, 5, 6, 7, 8, 1. Overlapping legs have been offset slightly to show the flight path.

Fig. 2. Boxcar cut-off sequence for leg 2-3 on 16 February 1986 for potential temperature variance.

Fig. 3. Spectral filter cut-off sequence for leg 2-3 on 16 February 1986 for potential temperature variance.

Fig. 4. Three dimensional representation of sea surface temperature on 16 February 1986.

Fig. 5. Boxcar average of potential temperature for all cross frontal legs on 16 February 1986.

Fig. 6. Boxcar average of specific humidity for all cross frontal legs on 16 February 1986.

Fig. 7. Boxcar potential temperature variance for all cross frontal legs on 16 February 1986.

Fig. 8. Boxcar vertical velocity variance for all cross frontal legs on 16 February 1986.

Fig. 9. Boxcar specific humidity variance for all cross frontal legs on 16 February 1986.

Fig. 10. The kinematic vertical heat flux for all cross frontal legs on 16 February 1986.

Fig. 11. The kinematic vertical specific humidity flux for all cross frontal legs on 16 February 1986.

Fig. 12. The kinematic vertical momentum flux for all cross frontal legs on 16 February 1986.

Fig. 13. Boxcar coherence between vertical velocity and potential temperature on 16 February 1986.

Fig. 14. Three dimensional representation of sea surface temperature on 17 February 1986.

Fig. 15. Boxcar average of potential temperature for all cross frontal legs on 17 February 1986.

Fig. 16. Boxcar average of specific humidity for all cross frontal legs on 17 February 1986.

Fig. 17. Boxcar potential temperature variance for all cross frontal legs on 17 February 1986.

Fig. 18. Boxcar vertical velocity variance for all cross frontal legs on 17 February 1986.

Fig. 19. Boxcar specific humidity variance for all cross frontal legs on 17 February 1986.

Fig. 20. The kinematic vertical heat flux for all cross frontal legs on 17 February 1986.

Fig. 21. Boxcar correlation between vertical velocity and potential temperature on 17 February 1986.

Fig. 22. The kinematic vertical specific humidity flux for all cross frontal legs on 17 February 1986.

Fig. 23. The kinematic vertical momentum flux for all cross frontal legs on 17 February 1986.

Fig. 24. Three dimensional representation of sea surface temperature on 18 February 1986.

Fig. 25. Boxcar average of potential temperature for all cross frontal legs on 18 February 1986.

Fig. 26. Boxcar average of specific humidity for all cross frontal legs on 18 February 1986.

Fig. 27. Boxcar potential temperature variance for all cross frontal legs on 18 February 1986.

Fig. 28. Boxcar vertical velocity variance for all cross frontal legs on 18 February 1986.

Fig. 29. Boxcar specific humidity variance for all cross frontal legs on 18 February 1986.

Fig. 30. The kinematic vertical heat flux for all cross frontal legs on 18 February 1986.

Fig. 31. The kinematic vertical specific humidity flux for all cross frontal legs on 18 February 1986.

Fig. 32. The kinematic vertical momentum flux for all cross frontal legs on 18 February 1986.

Fig. 33. Boxcar correlation between vertical velocity and potential temperature on 18 February 1986.

The FASINEX Flight Box.

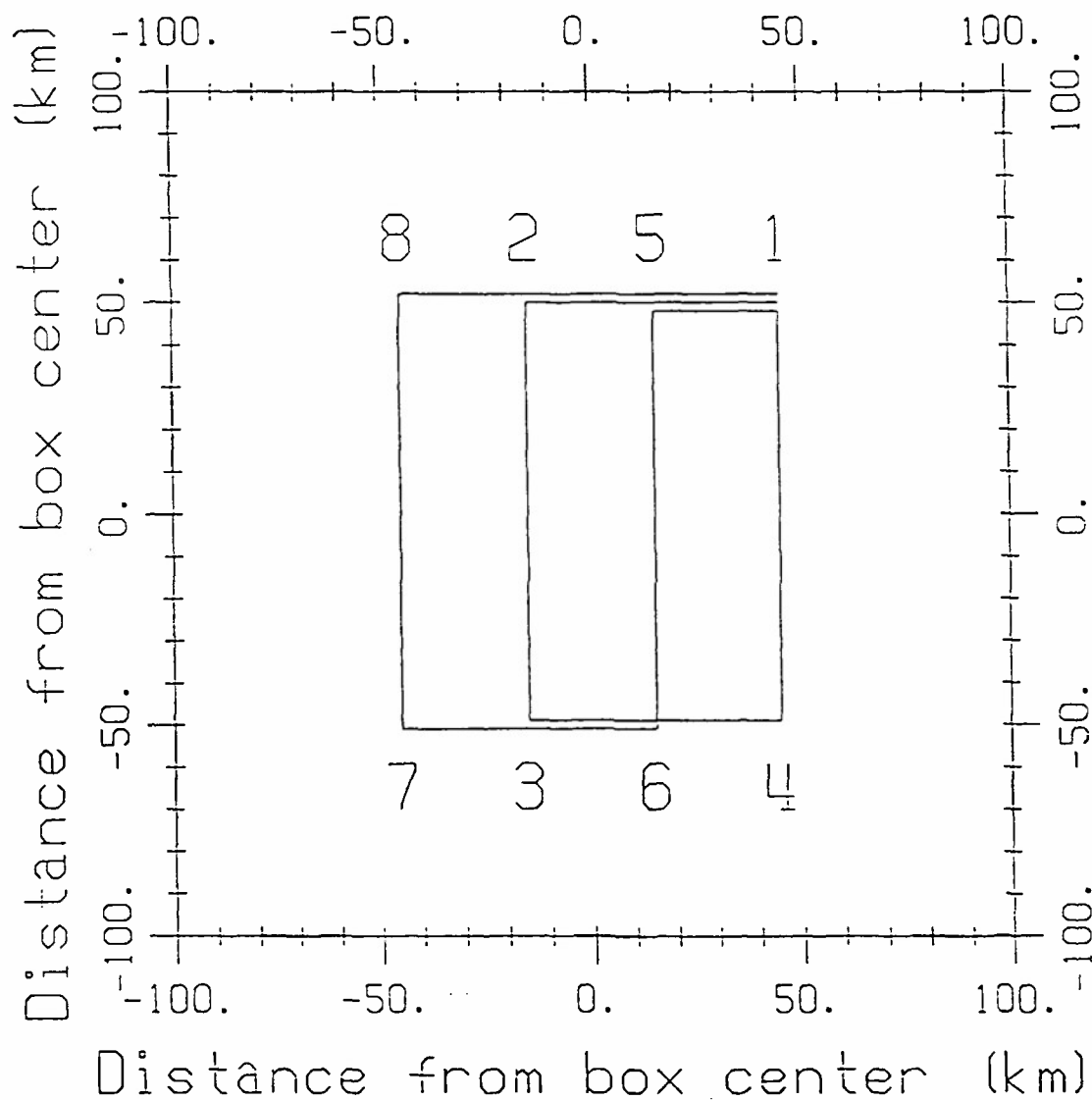


Fig. 1. The FASINEX flight box. The box was flown from in the order 1, 2, 3, 4, 1, 5, 6, 7, 8, 1. Overlapping legs have been offset slightly to show the flight path.

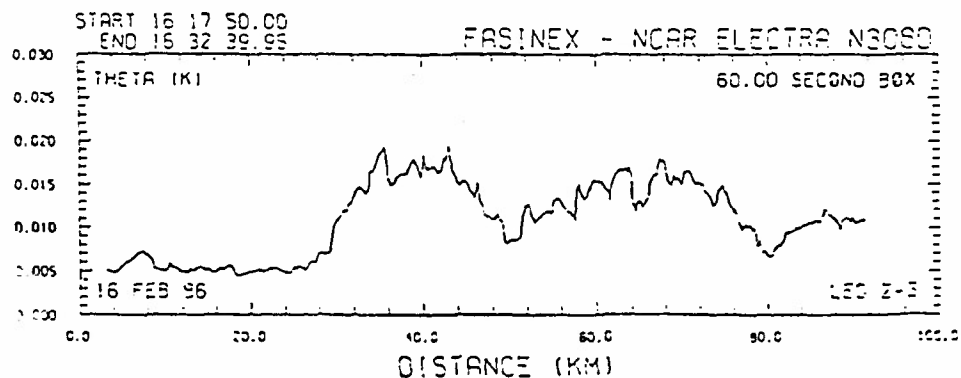
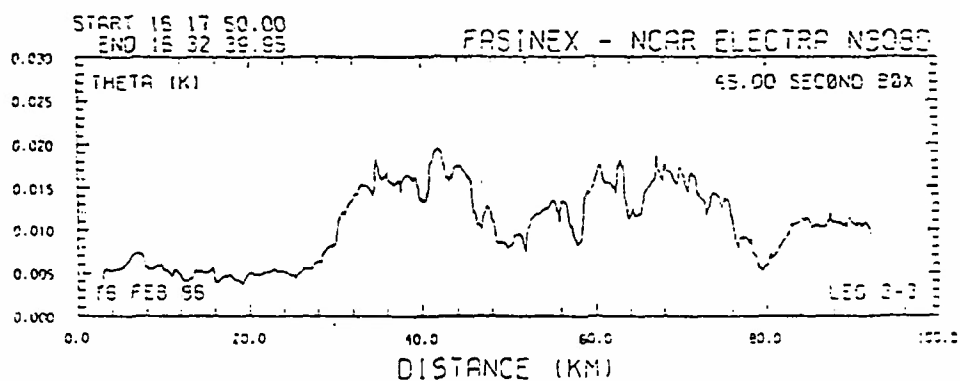
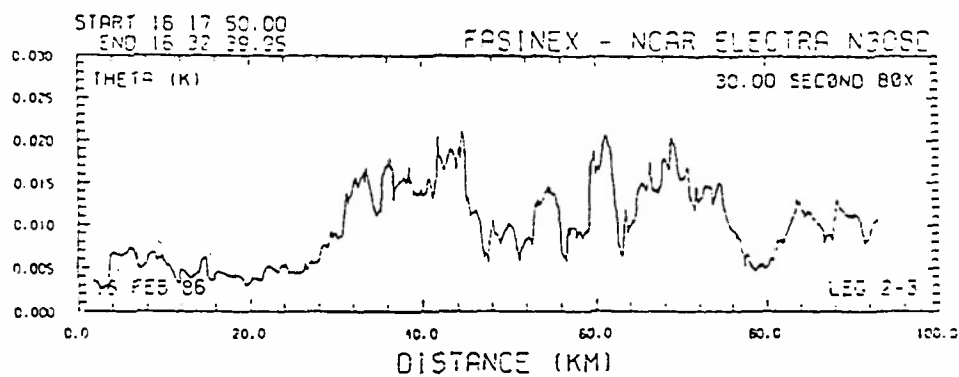
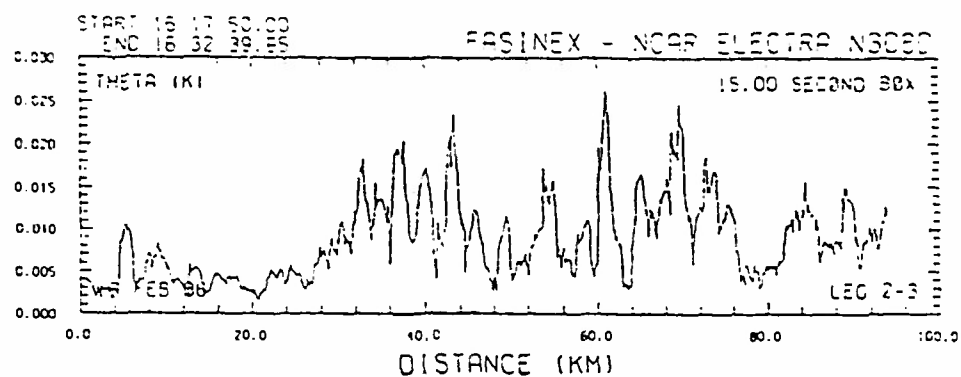


Figure 2

Boxcar Cut Off Sequence
16 FEB 86 Potential Temperature Leg 2-3

Fig. 2. Boxcar cut-off sequence for leg 2-3 on 16 February 1986 for potential temperature variance.

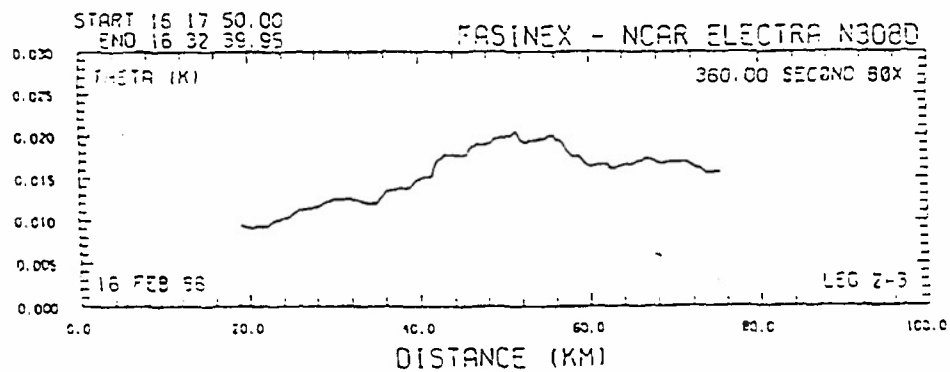
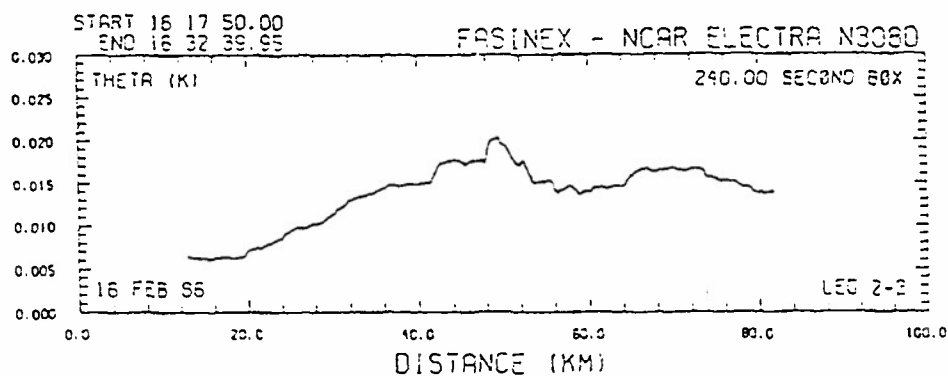
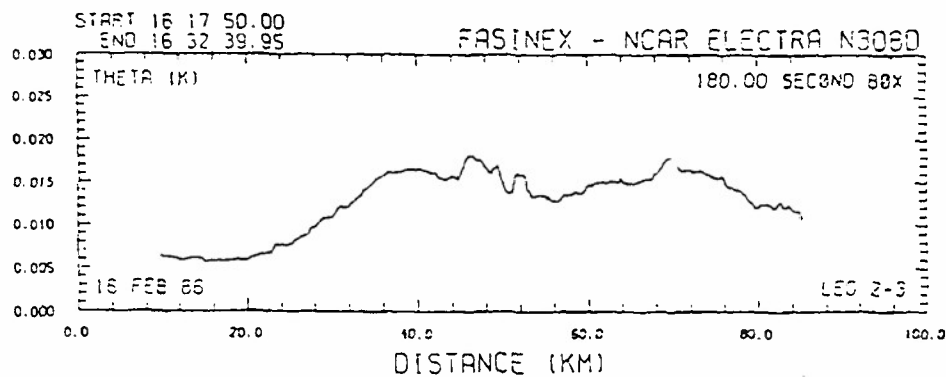
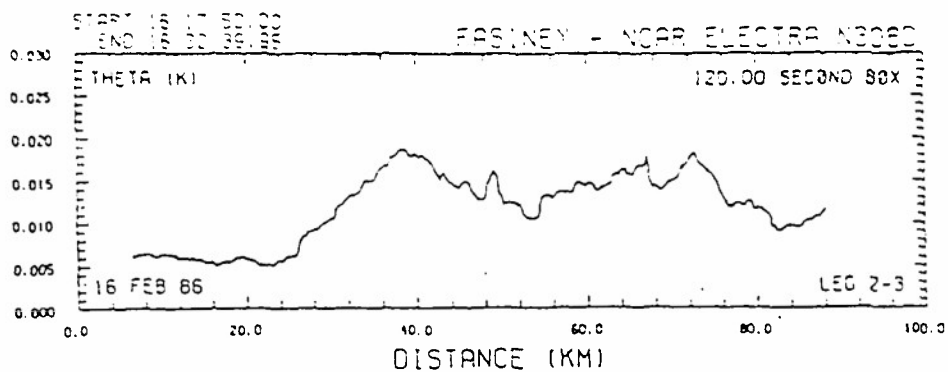


Figure 2 (cont.)

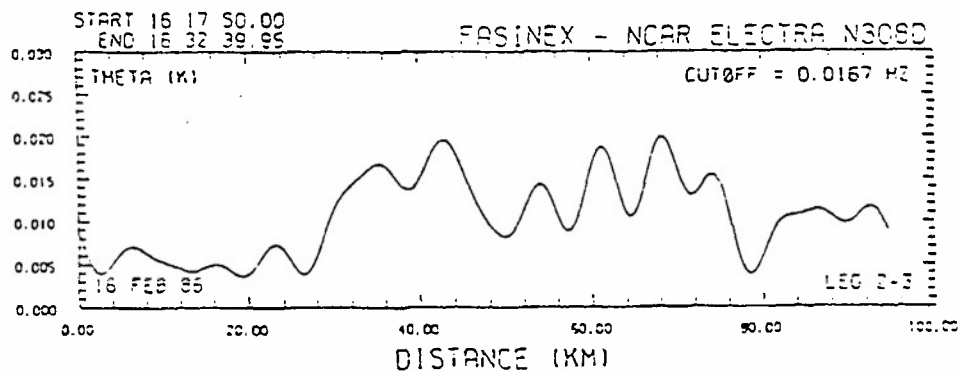
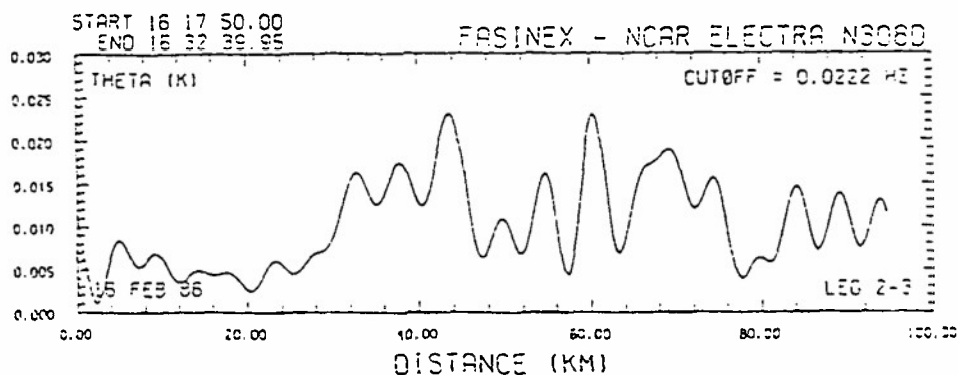
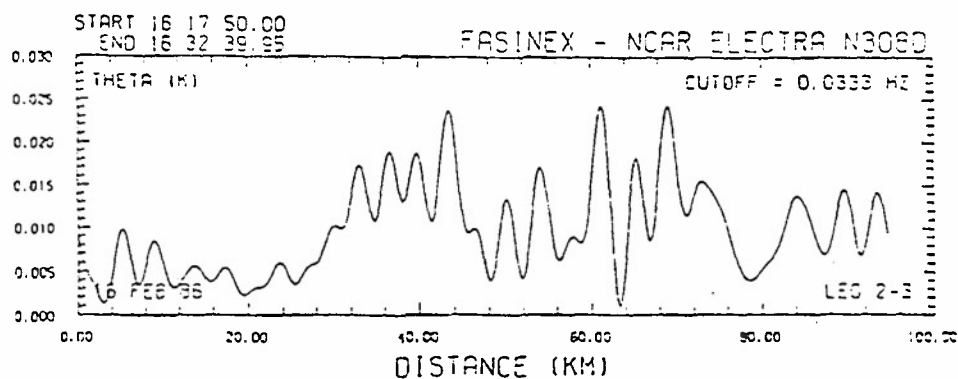
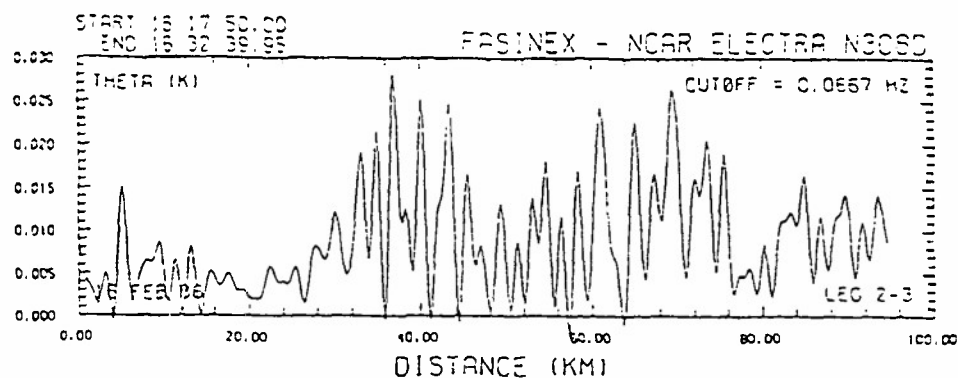


Figure 3

Spectral Filter Cut Off Sequence
16 FEB 86 Potential Temperature Leg 2-3

Fig. 3. Spectral filter cut-off sequence for leg 2-3 on 16 February 1986 for potential temperature variance.

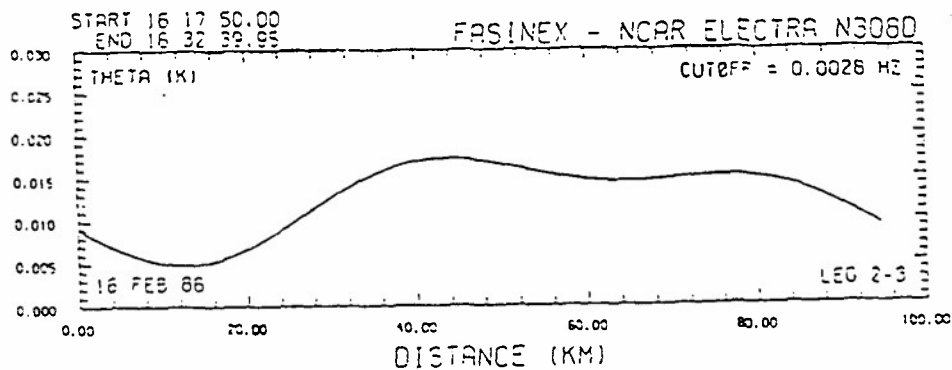
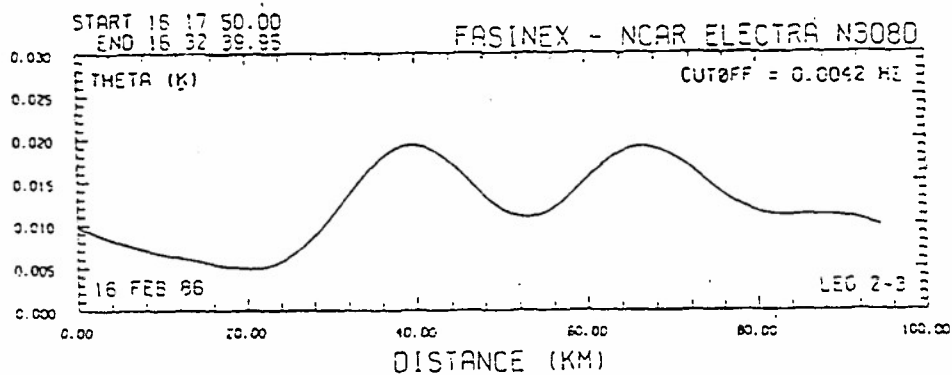
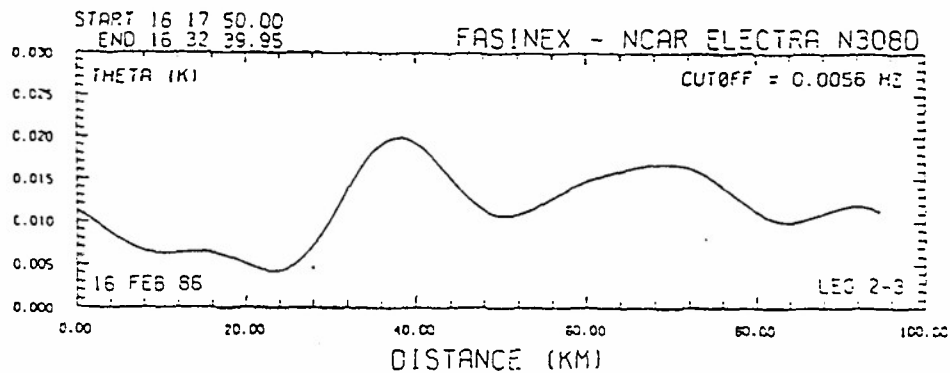
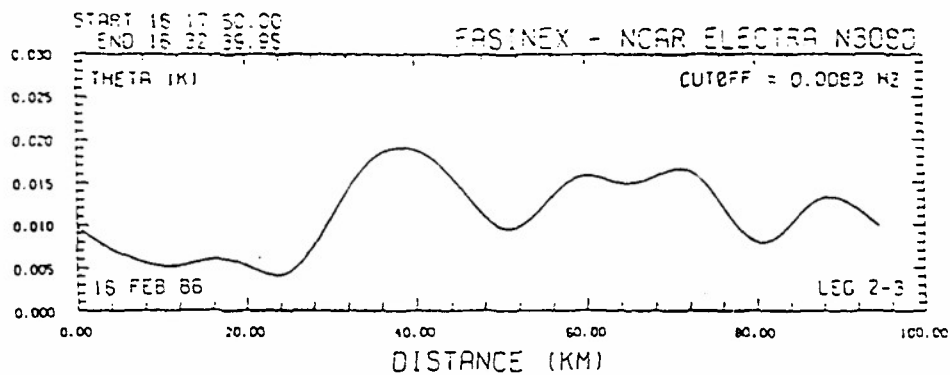
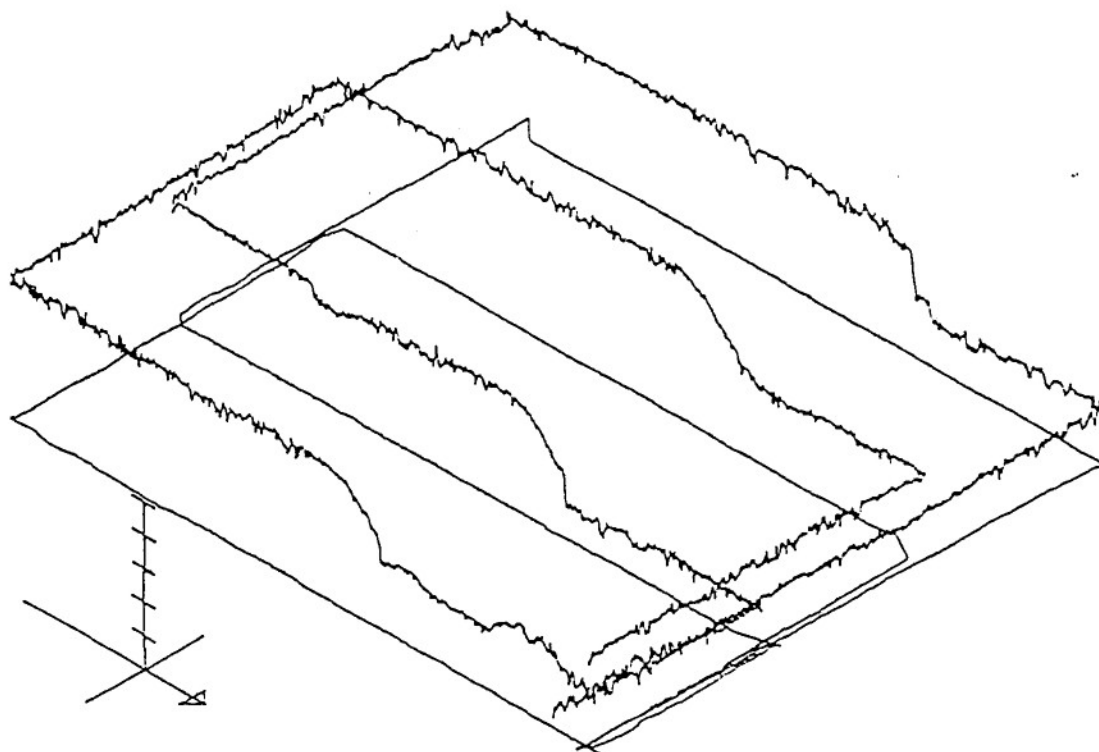


Figure 3 (cont.)



Z AXIS MAX = 24.00
Z AXIS MIN = 19.00
Z INC = 1.00

Z MAX = 23.62
Z MIN = 19.71

16 FEB 86
SST (C)

Fig. 4. Three dimensional representation of sea surface temperature on 16 February 1986.

FASINEX - NCAR ELECTRA N308D THETA (K)

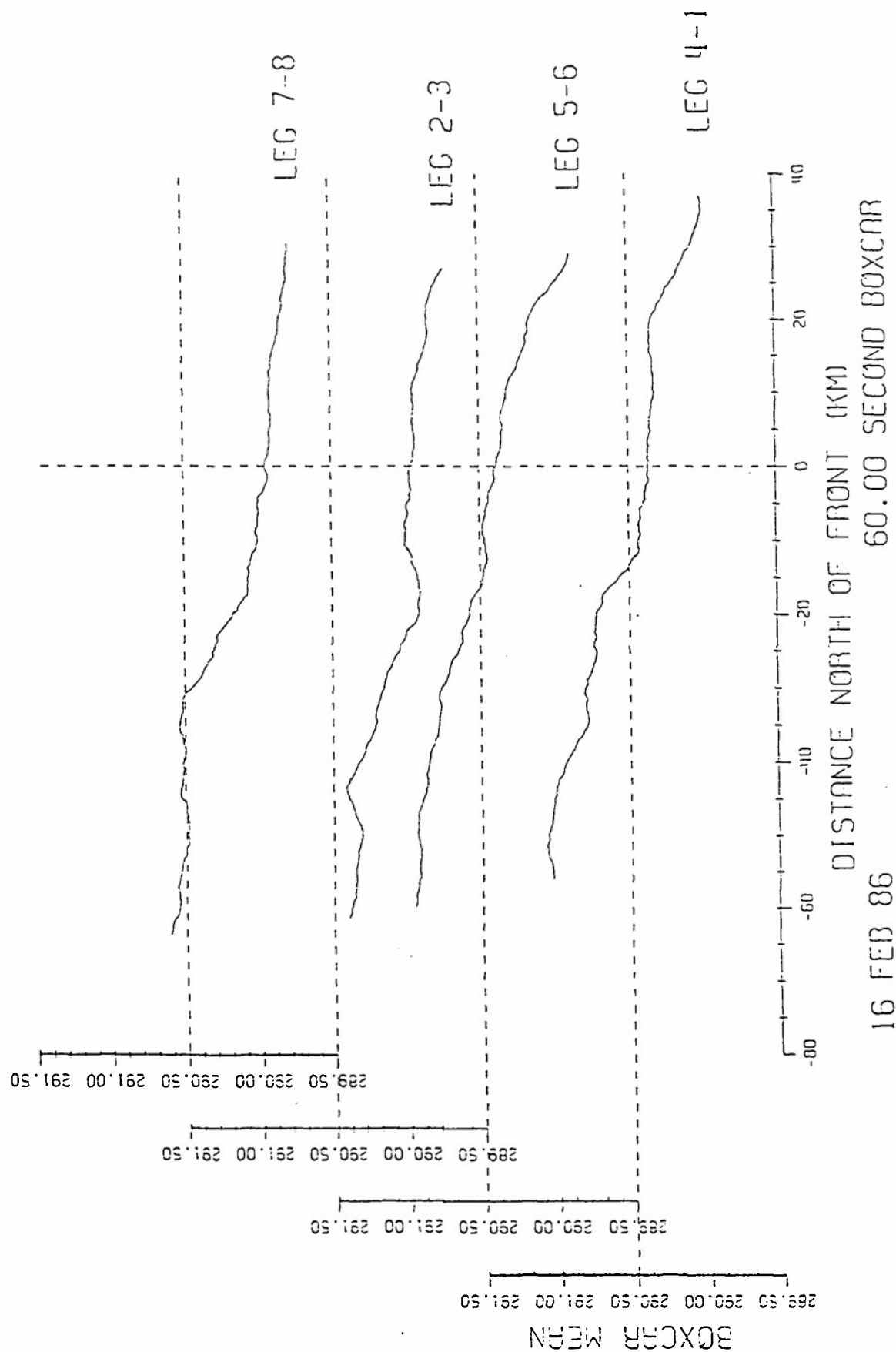


Fig. 5. Boxcar average of potential temperature for all cross frontal legs on 16 February 1986.

FASINEX - NCAR ELECTRA N308D Q (g/kg)

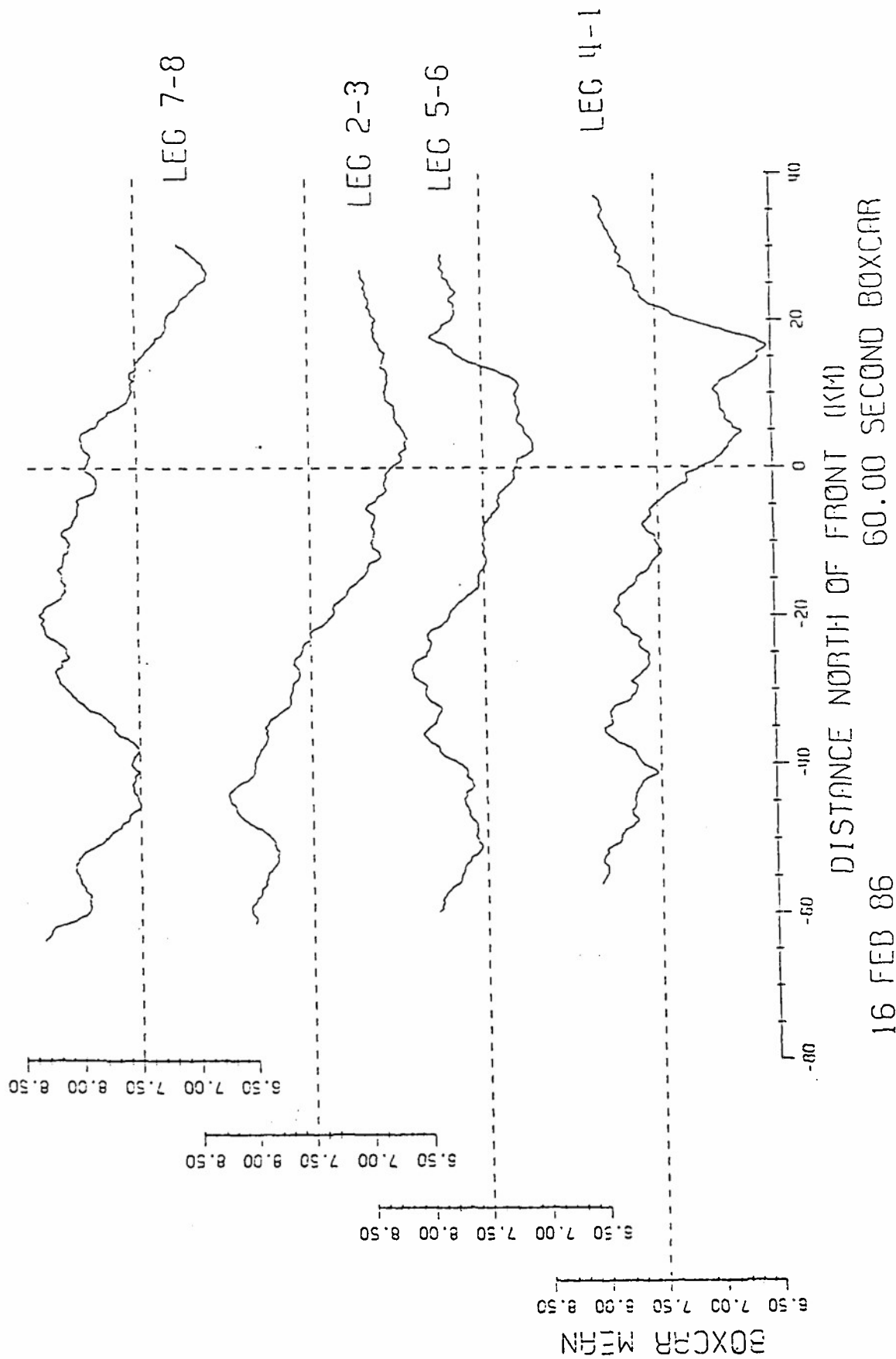


Fig. 6. Boxcar average of specific humidity for all cross frontal legs on 16 February 1986.

FASINEX - NCAR ELECTRA N308D THETA (K)

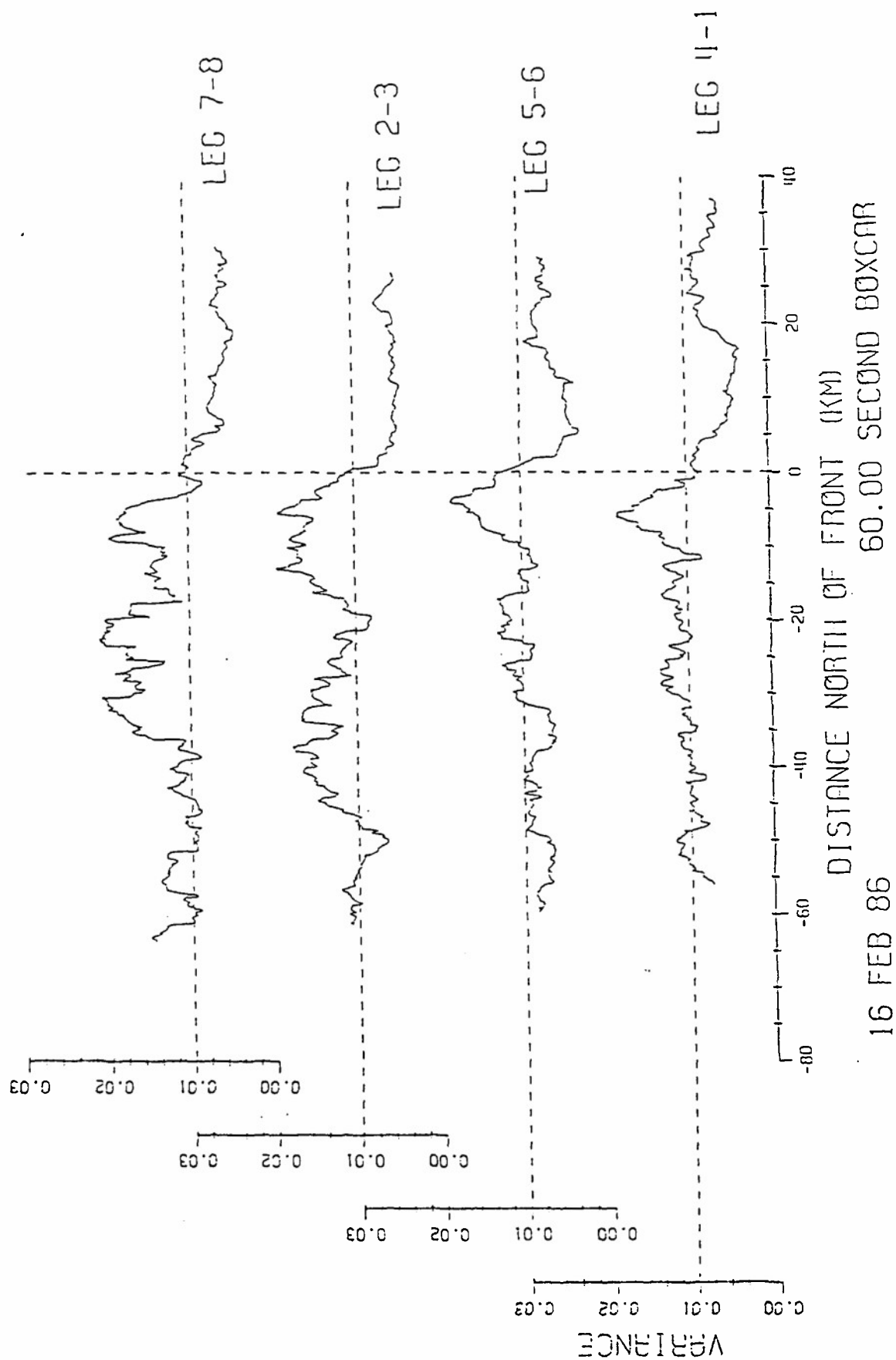


Fig. 7. Boxcar potential temperature variance for all cross frontal legs on 16 February 1986.

FASINEX - NCAR ELECTRA N308D W (m/s)

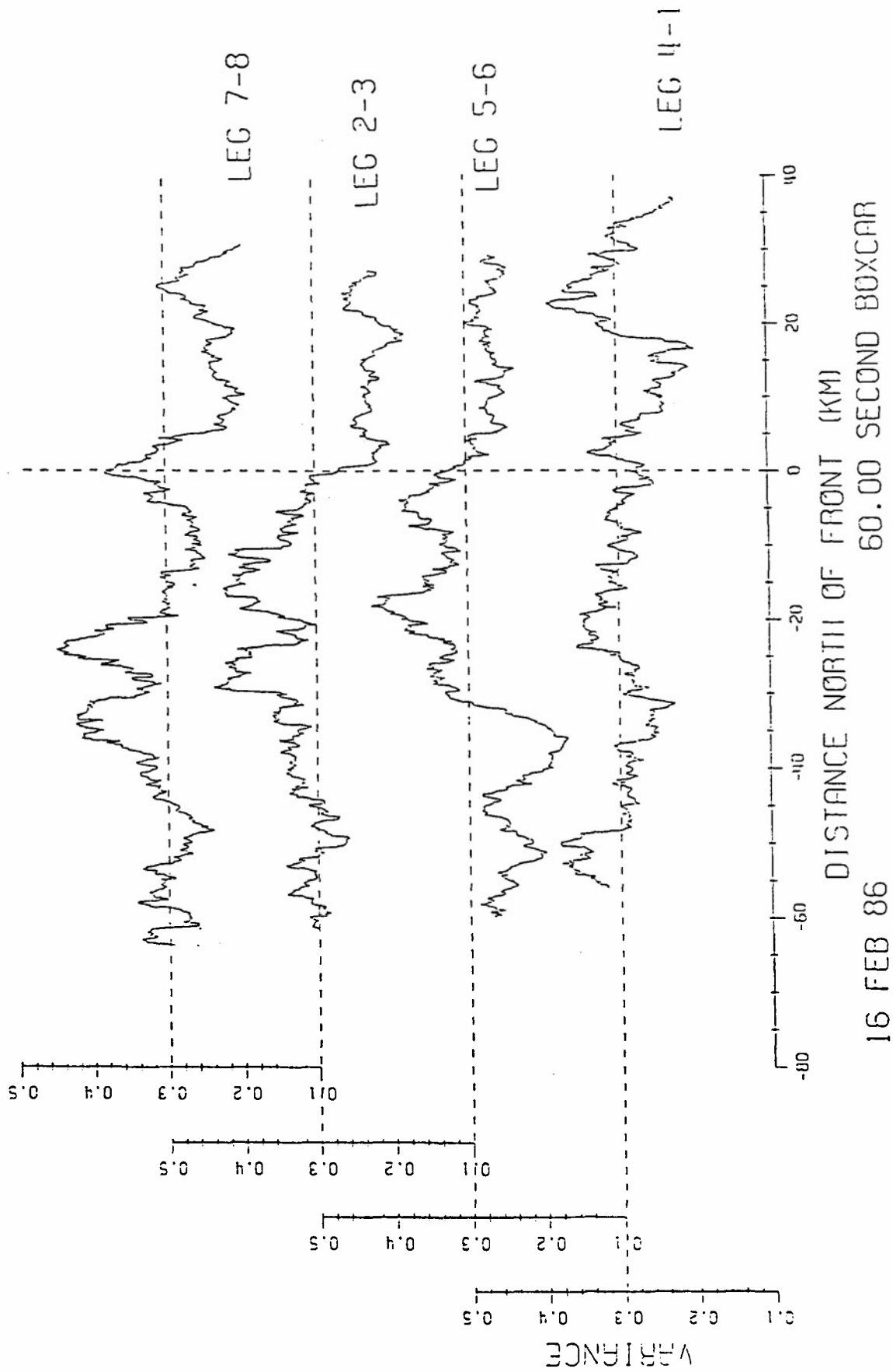


Fig. 8. Boxcar vertical velocity variance for all cross frontal legs on 16 February 1986.

FASINEX - NCAR ELECTRA N308D

Q (g/kg)

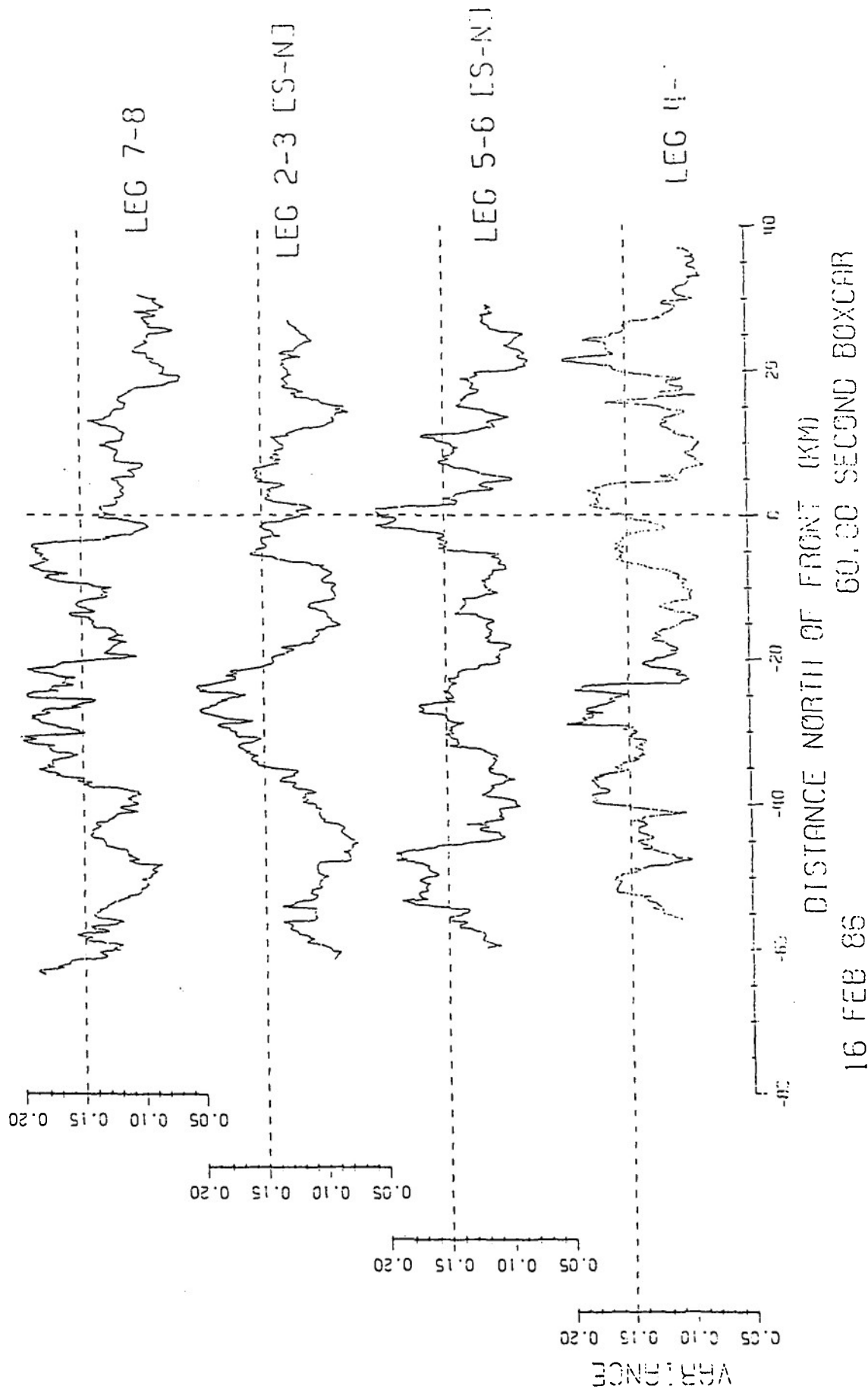


Fig. 9. Boxcar specific humidity variance for all cross frontal legs on 16 February 1986.

FASINEX - NCAR ELECTRA N308D
W (m/s)
THETA (K)

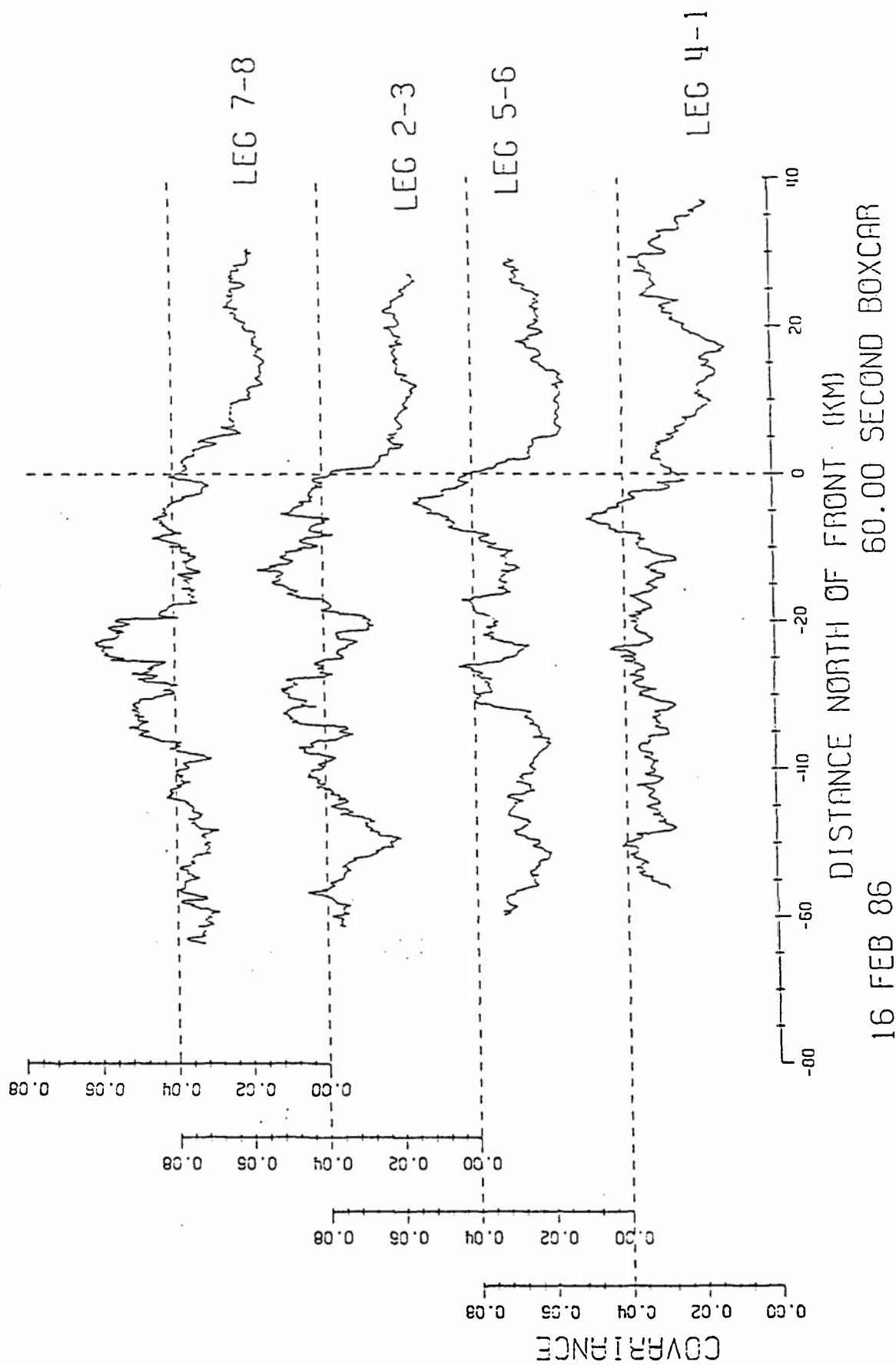


Fig. 10. The kinematic vertical heat flux for all cross frontal legs on 16 February 1986.

FASINEX - NCAR ELECTRA N308D
W (m/s)
Q (g/kg)

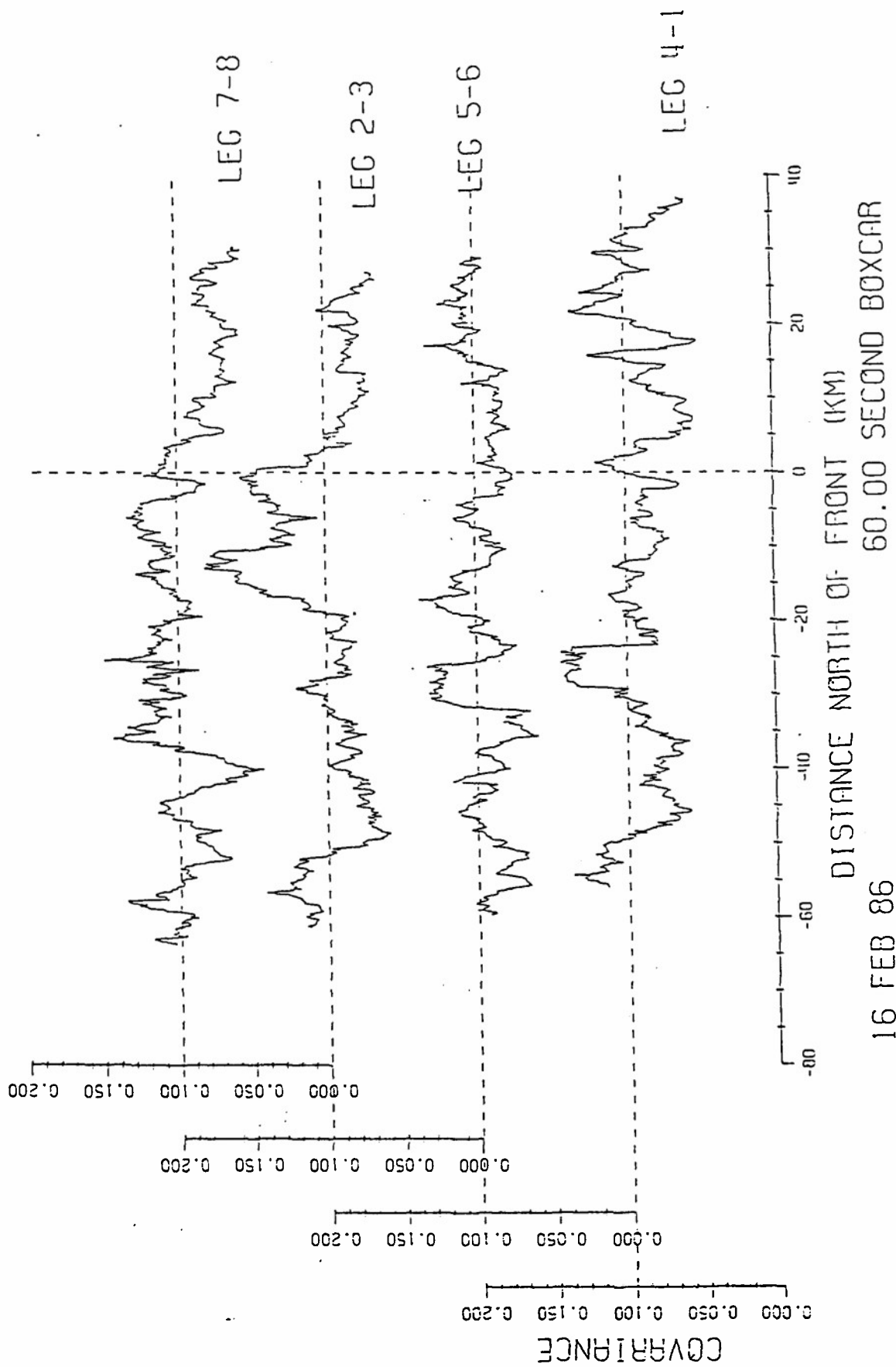


Fig. 11. The kinematic vertical specific humidity flux for all cross frontal legs on 16 February 1986.

FASINEX - NCAR ELECTRA N308D
 U (m/s) W (m/s)

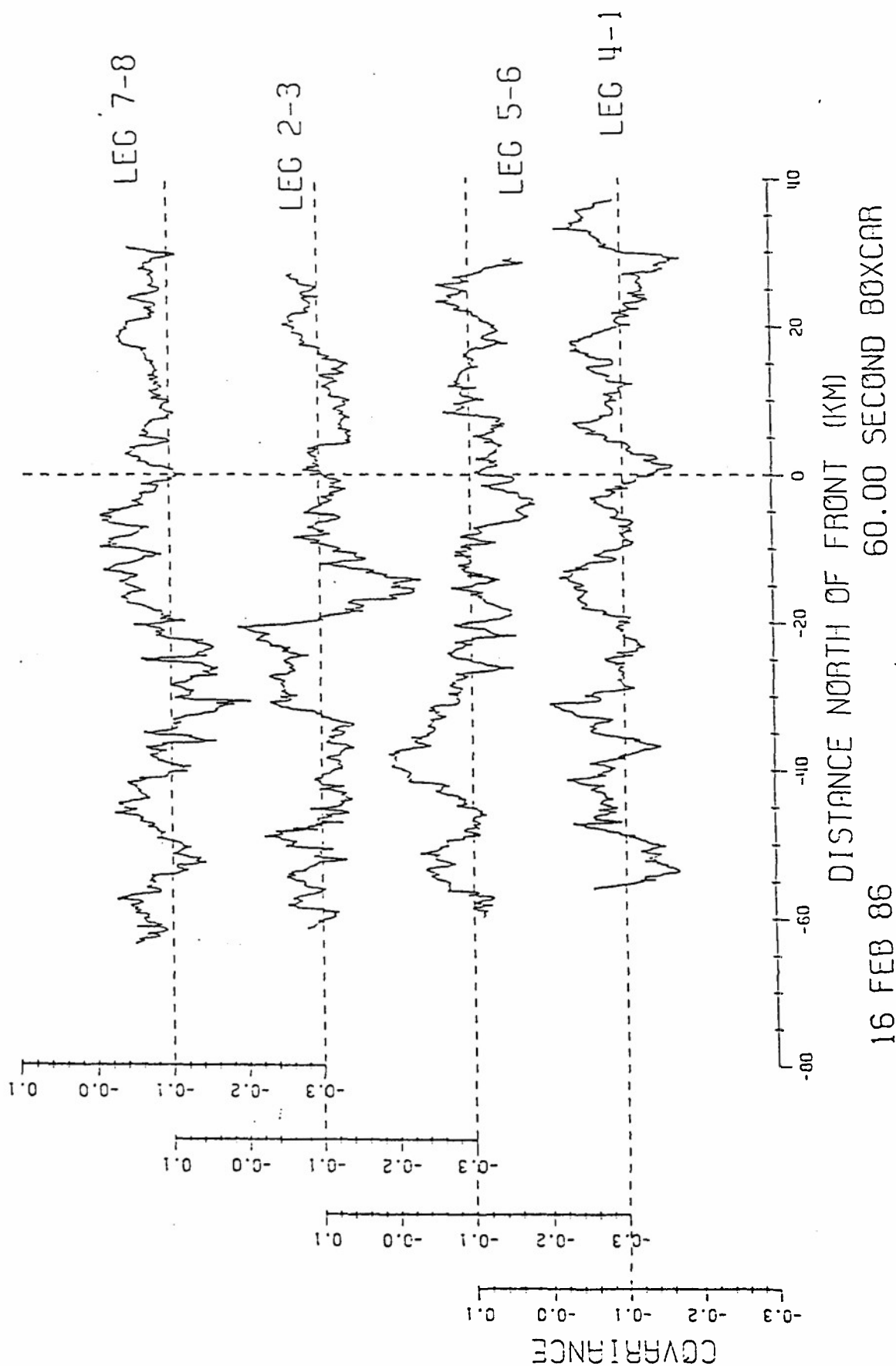


Fig. 12. The kinematic vertical momentum flux for all cross frontal legs on 16 February 1986.

FASINEX - NCAR ELECTRA N308D
W (m/s)
THETA (K)

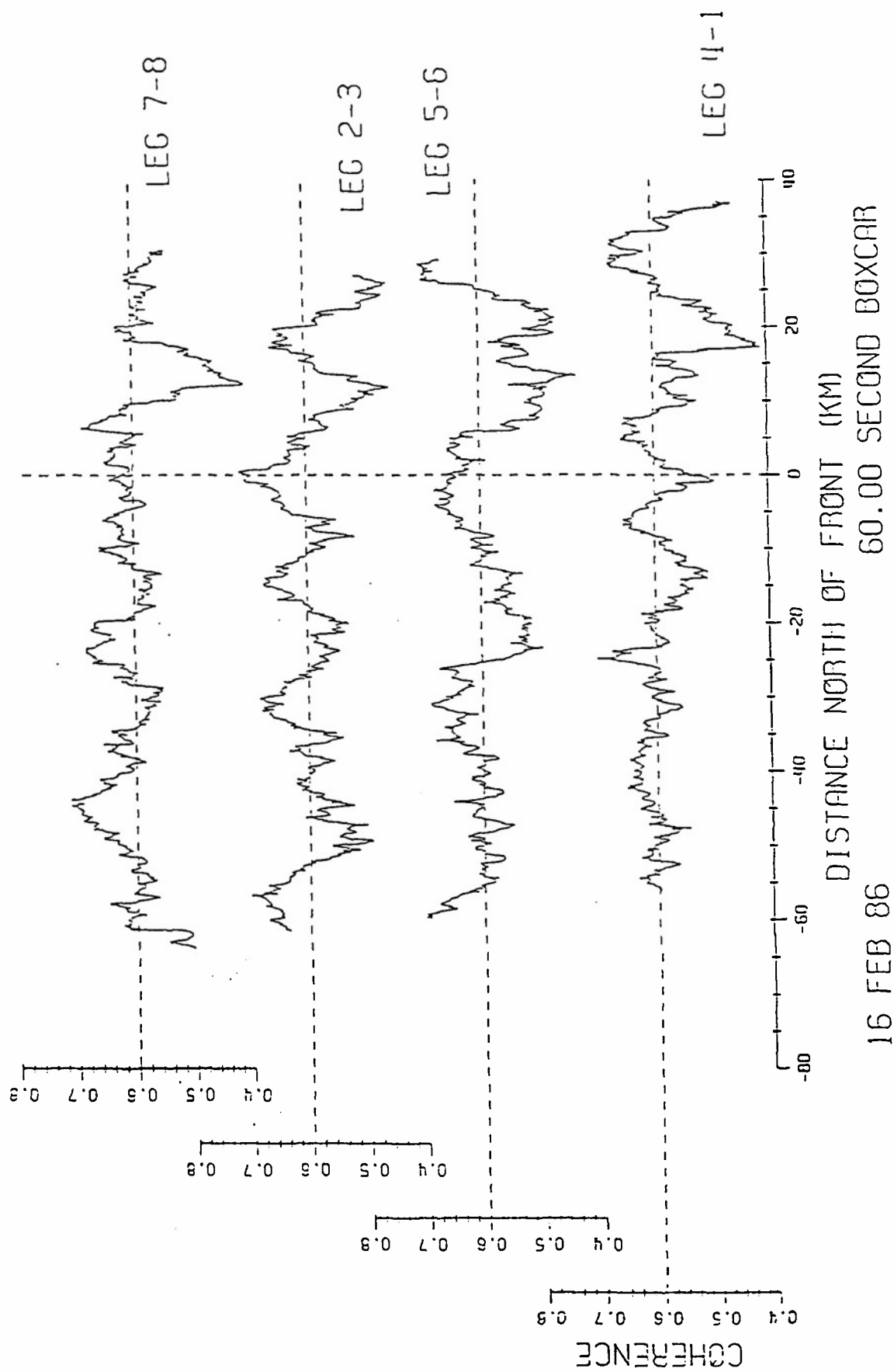
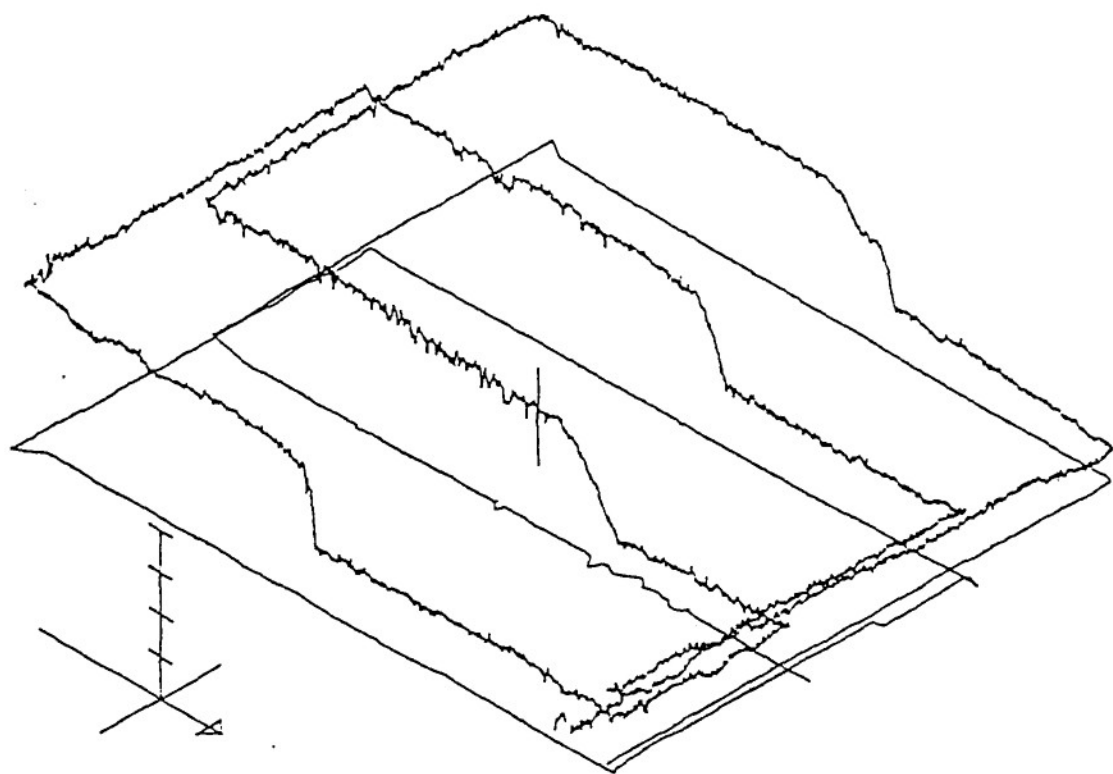


Fig. 13. Boxcar coherence between vertical velocity and potential temperature on 16 February 1986.



Z AXIS MAX = 28.00
 Z AXIS MIN = 19.00
 Z INC = 1.00

Z MAX = 22.82
 Z MIN = 19.57

16 FEB 86
 SST (C)

Fig. 14. Three dimensional representation of sea surface temperature on 17 February 1986.

FASINEX - NCAR ELECTRA N308D THETA (K)

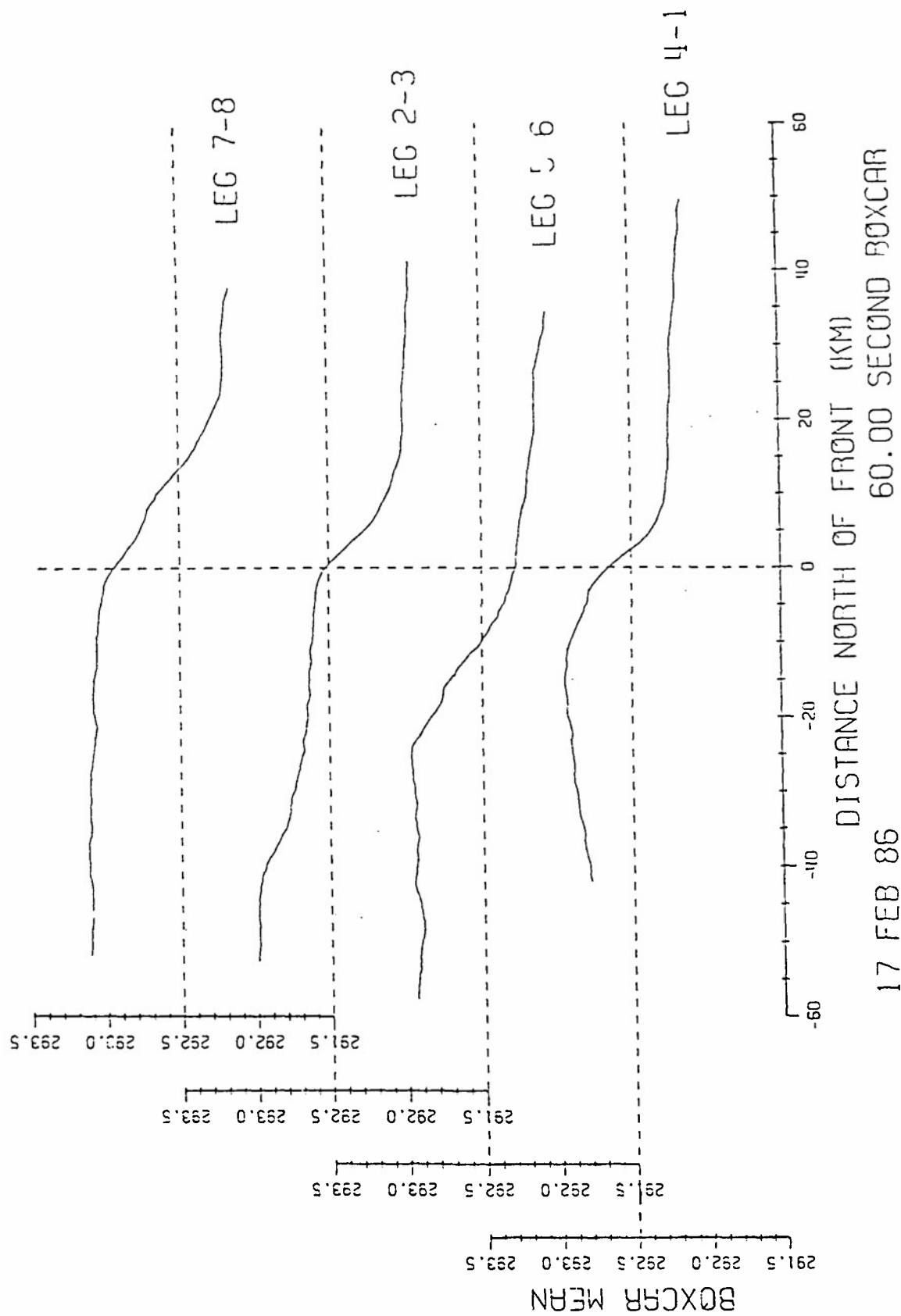


Fig. 15. Boxcar average of potential temperature for all cross frontal legs on 17 February 1986.

FASINEX - NCAR ELECTRA N308D
Q (g/kg)

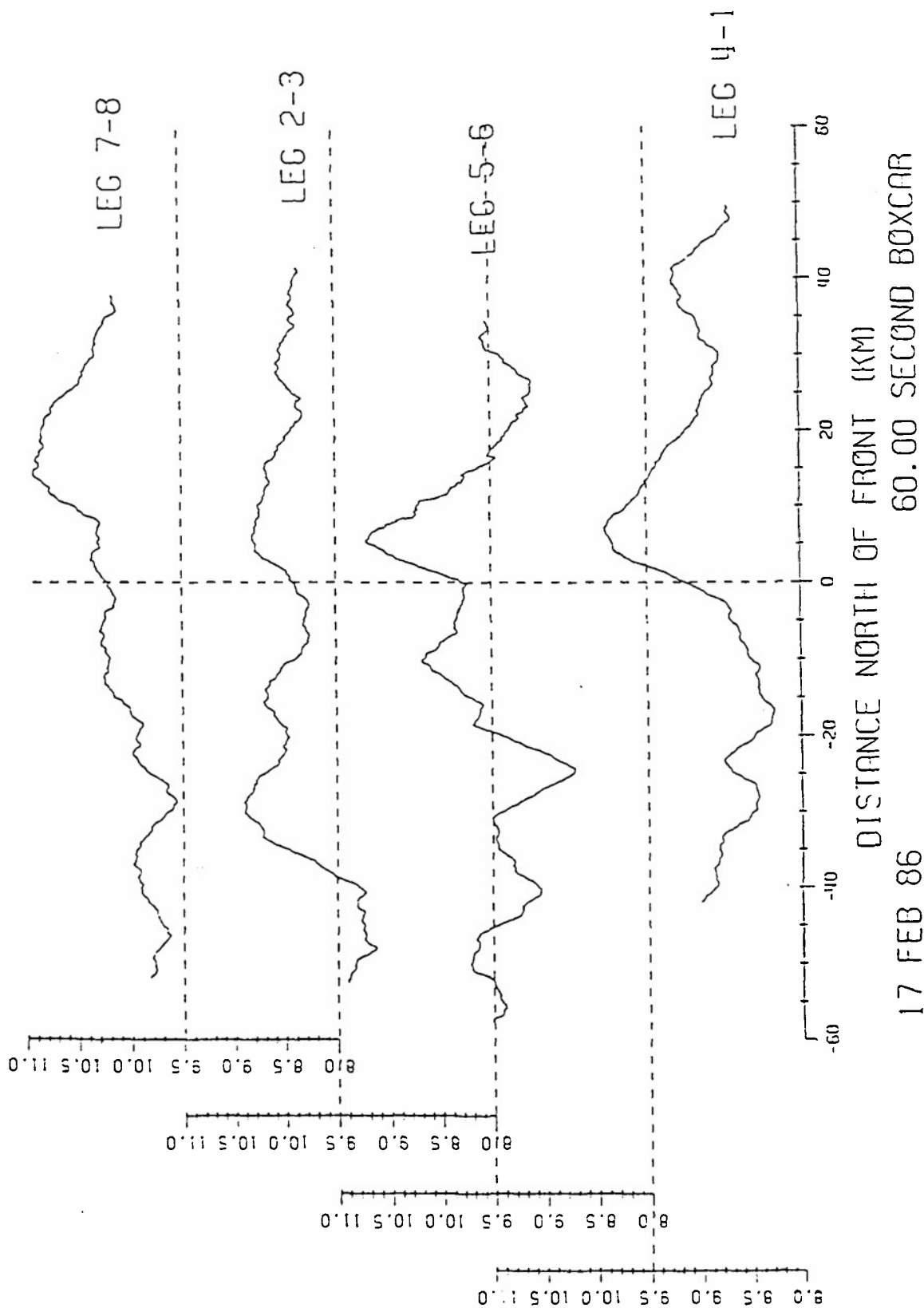


Fig. 16. Boxcar average of specific humidity for all cross frontal legs on 17 February 1986.

FASINEX - NCAR ELECTRA N308D
THETA (K)

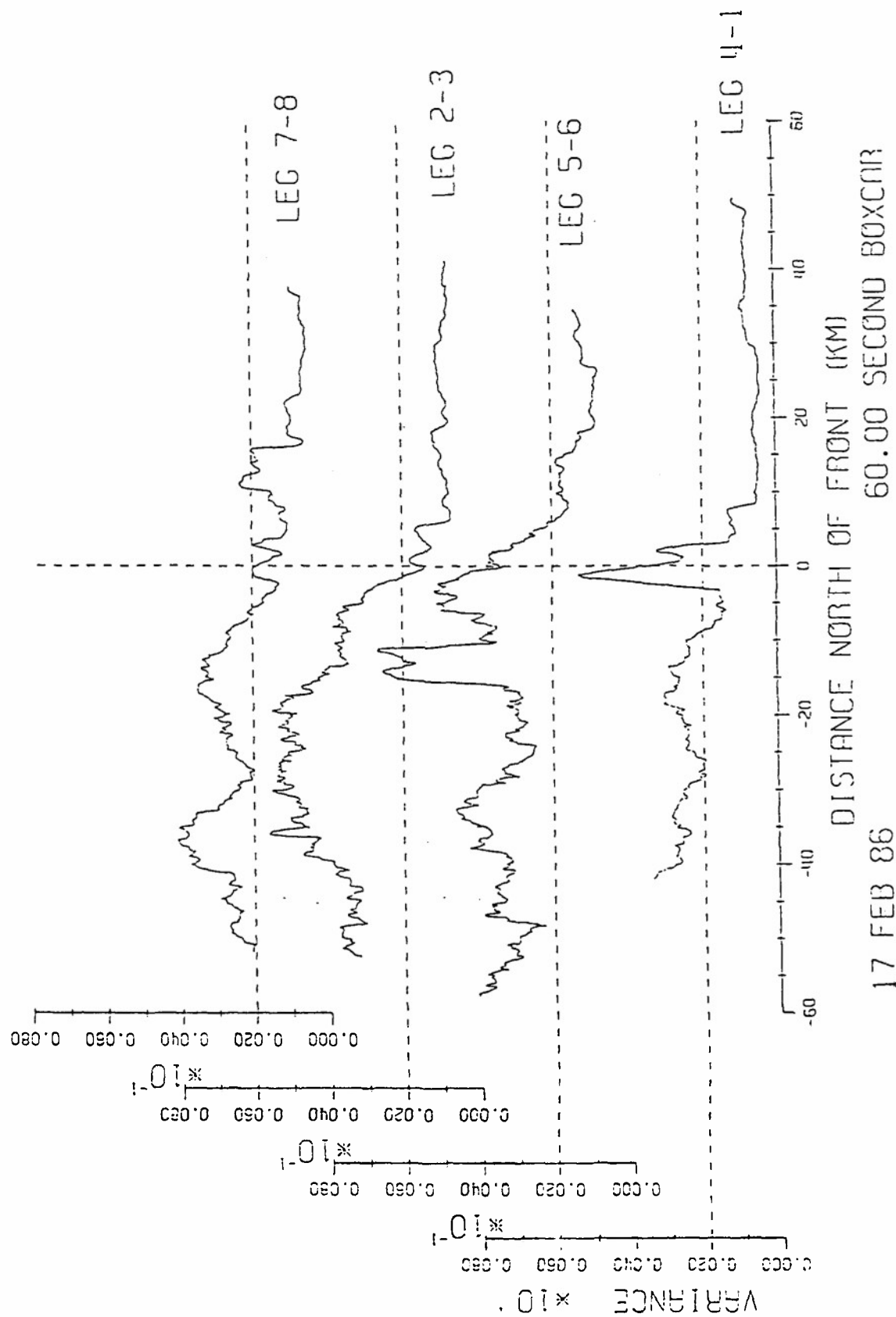


Fig. 17. Boxcar potential temperature variance for all cross frontal legs on 17 February 1986.

FASINEX - NCAR ELECTRA N308D
W (m/s)

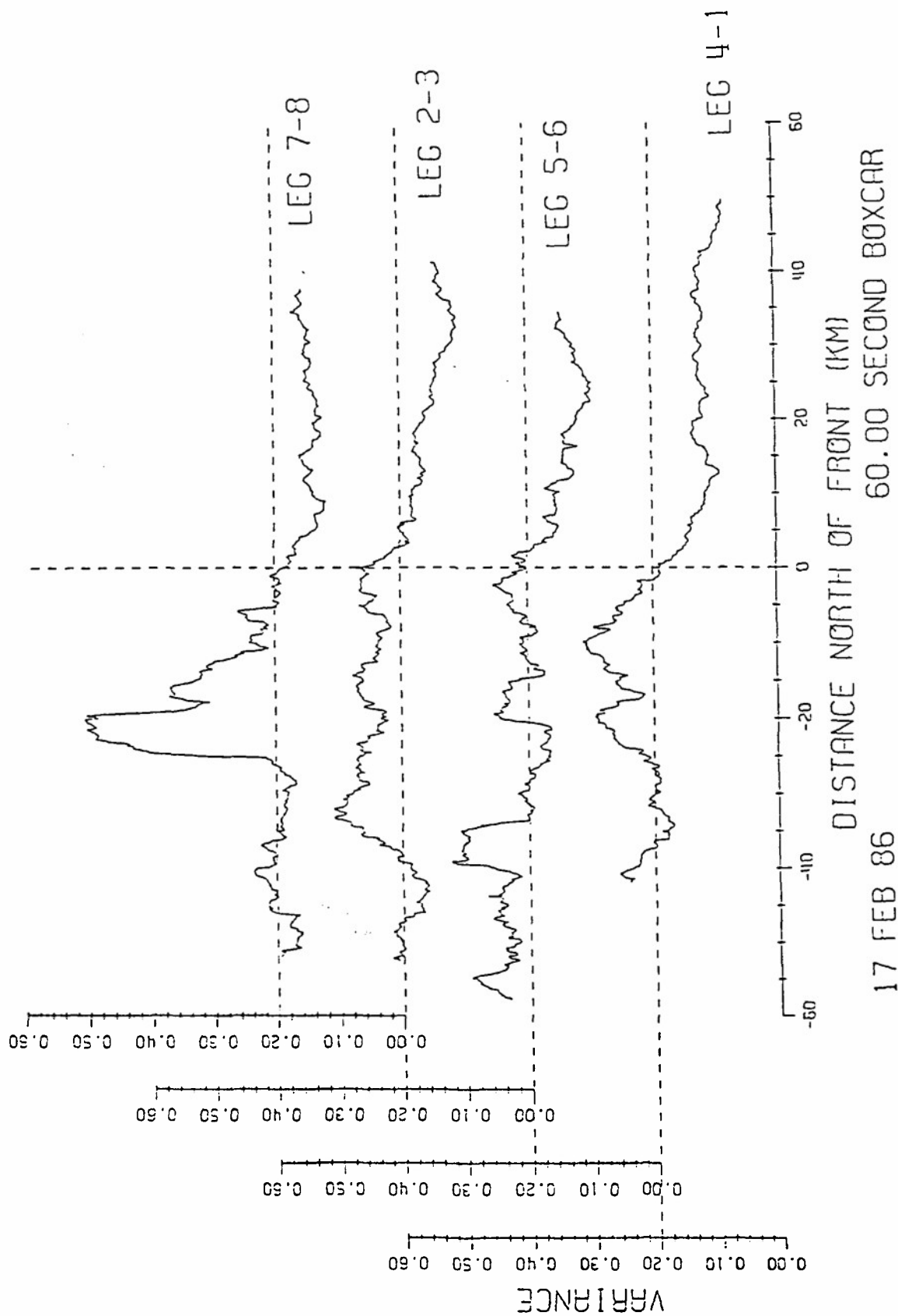


Fig. 18. Boxcar vertical velocity variance for all cross frontal legs on 17 February 1986.

FASINEX - NCAR ELECTRA N308D
Q (g/kg)

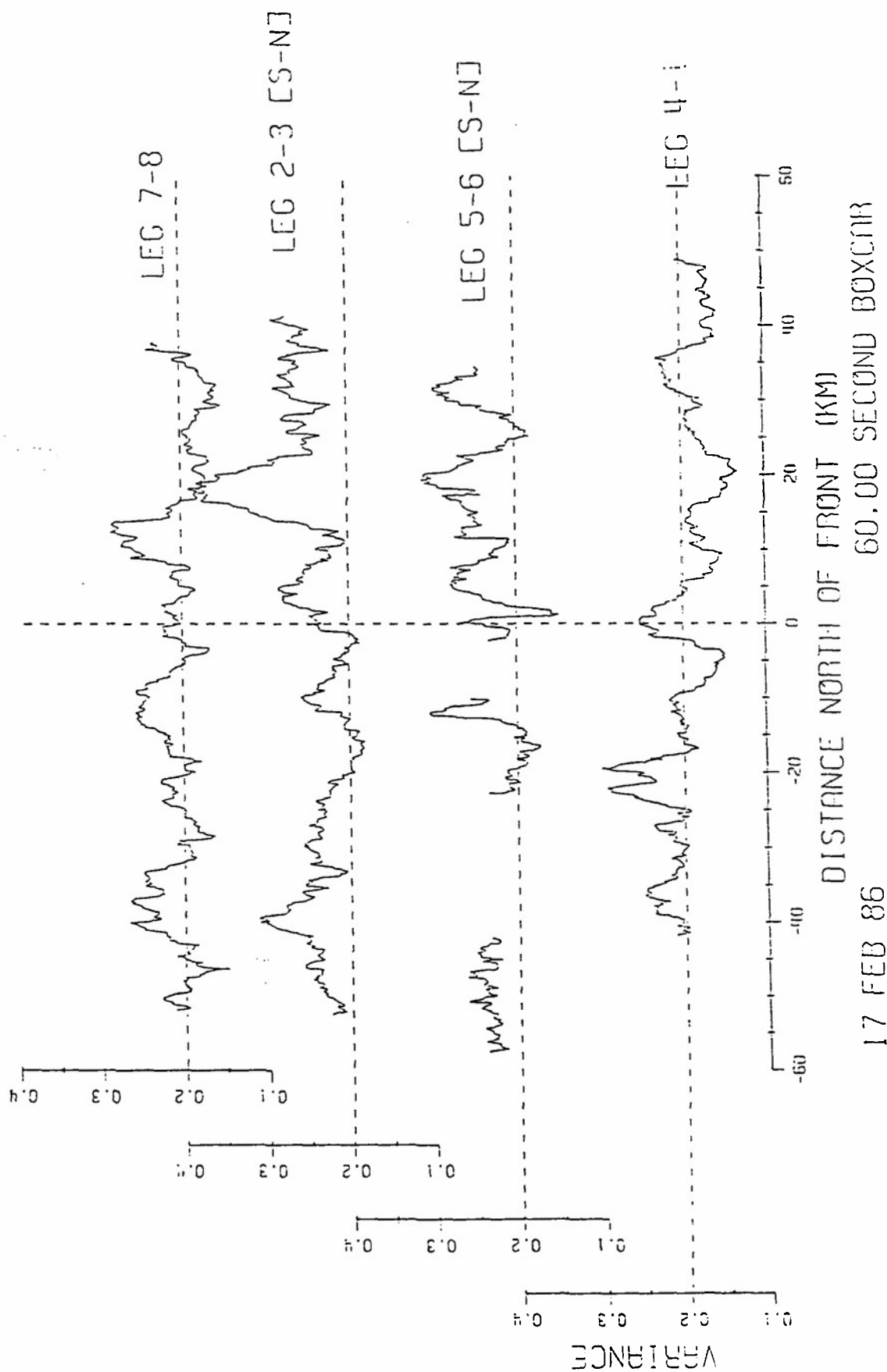


Fig. 19. Boxcar specific humidity variance for all cross frontal legs on 17 February 1986.

FASINEX - NCAR ELECTRA N308D
W (m/s)
THETA (K)

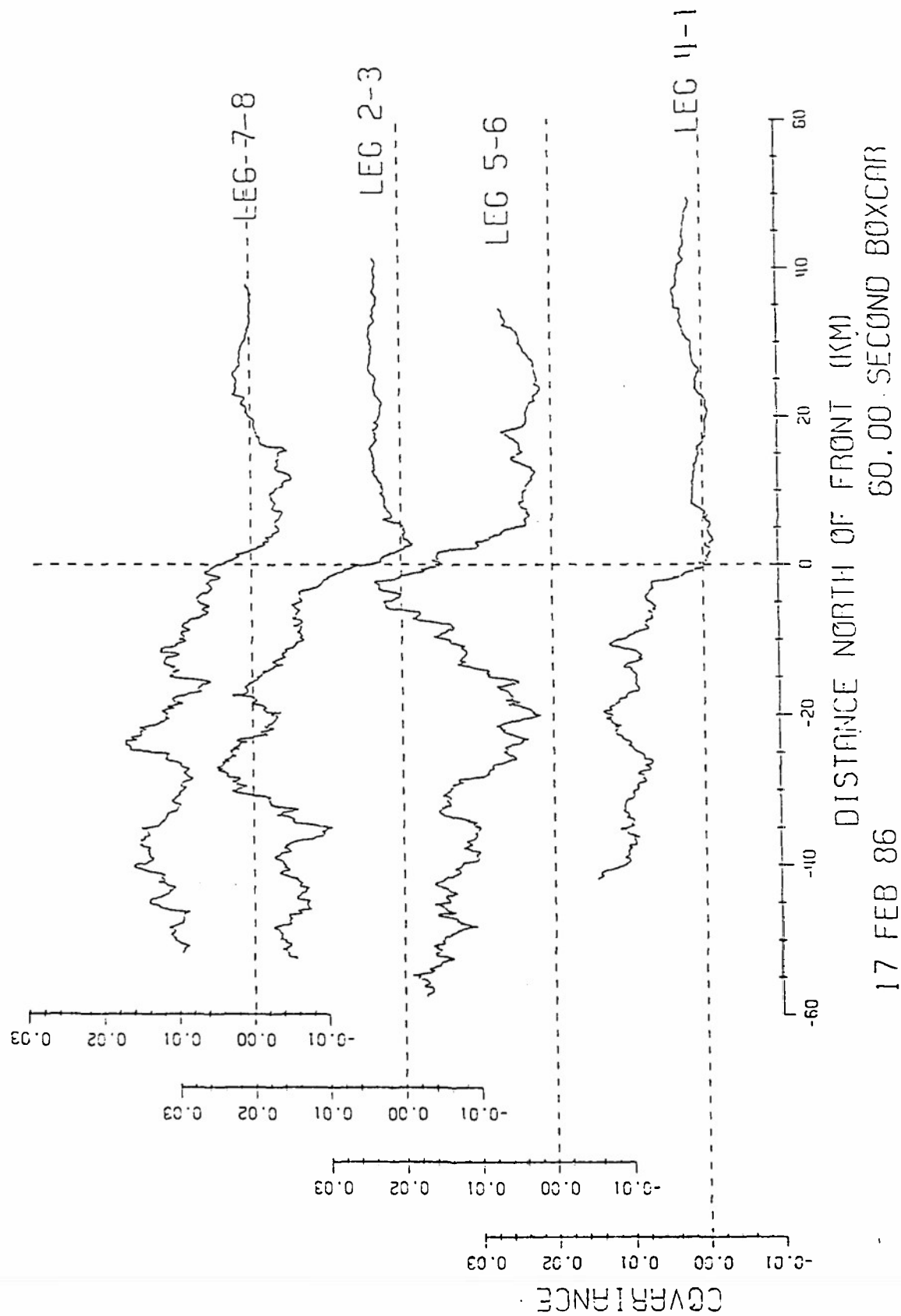
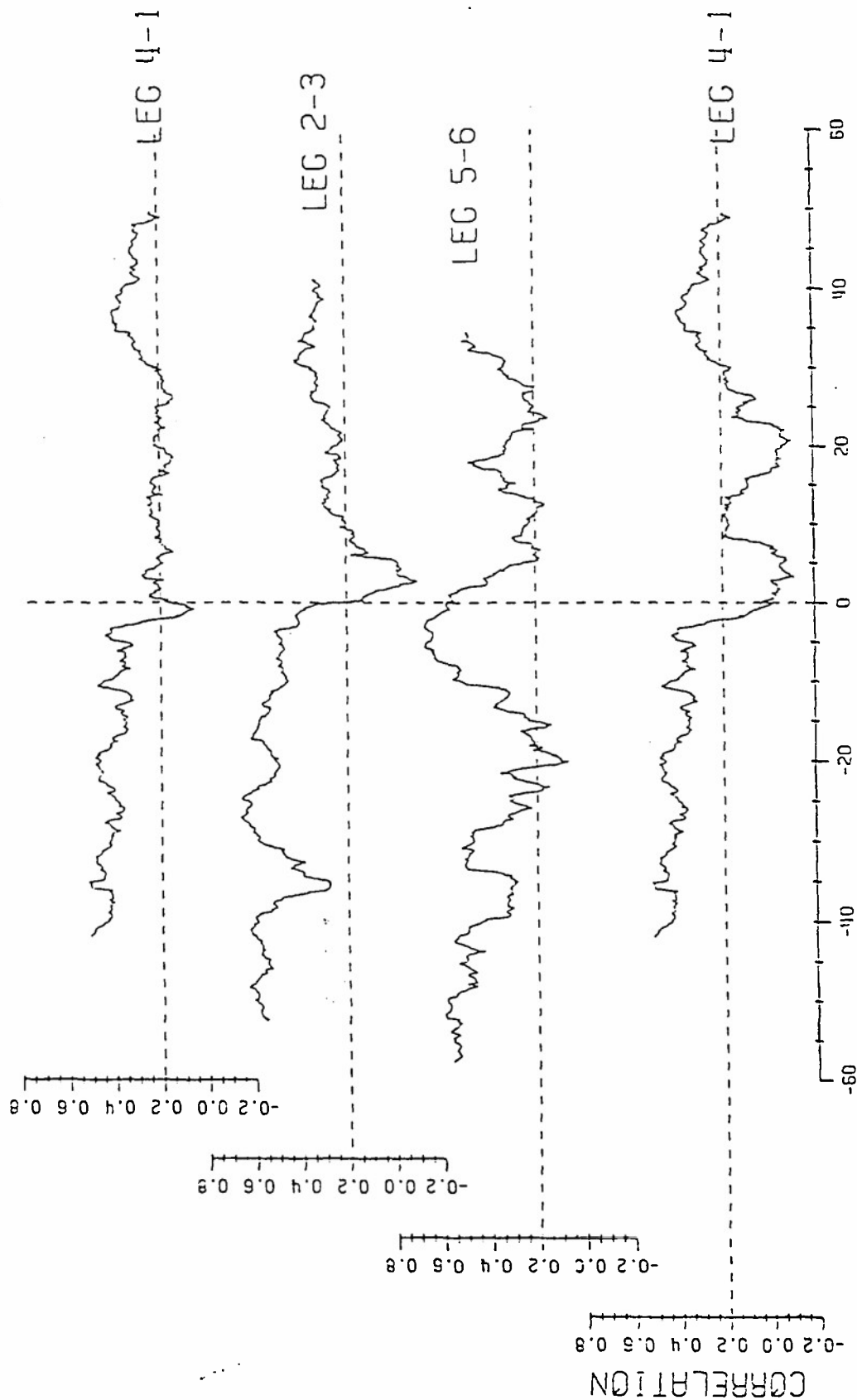


Fig. 20. The kinematic vertical heat flux for all cross frontal legs on 17 February 1986.

FASINEX - NCAR ELECTRA N308D
W (m/s)
THETA (K)



17 FEB 86
DISTANCE NORTH OF FRONT (KM)
60.00 SECOND BOXCAR

Fig. 21. Boxcar correlation between vertical velocity and potential temperature on 17 February 1986.

FASINEX - NCAR ELECTRA N308D
W (m/s) Q (g/kg)

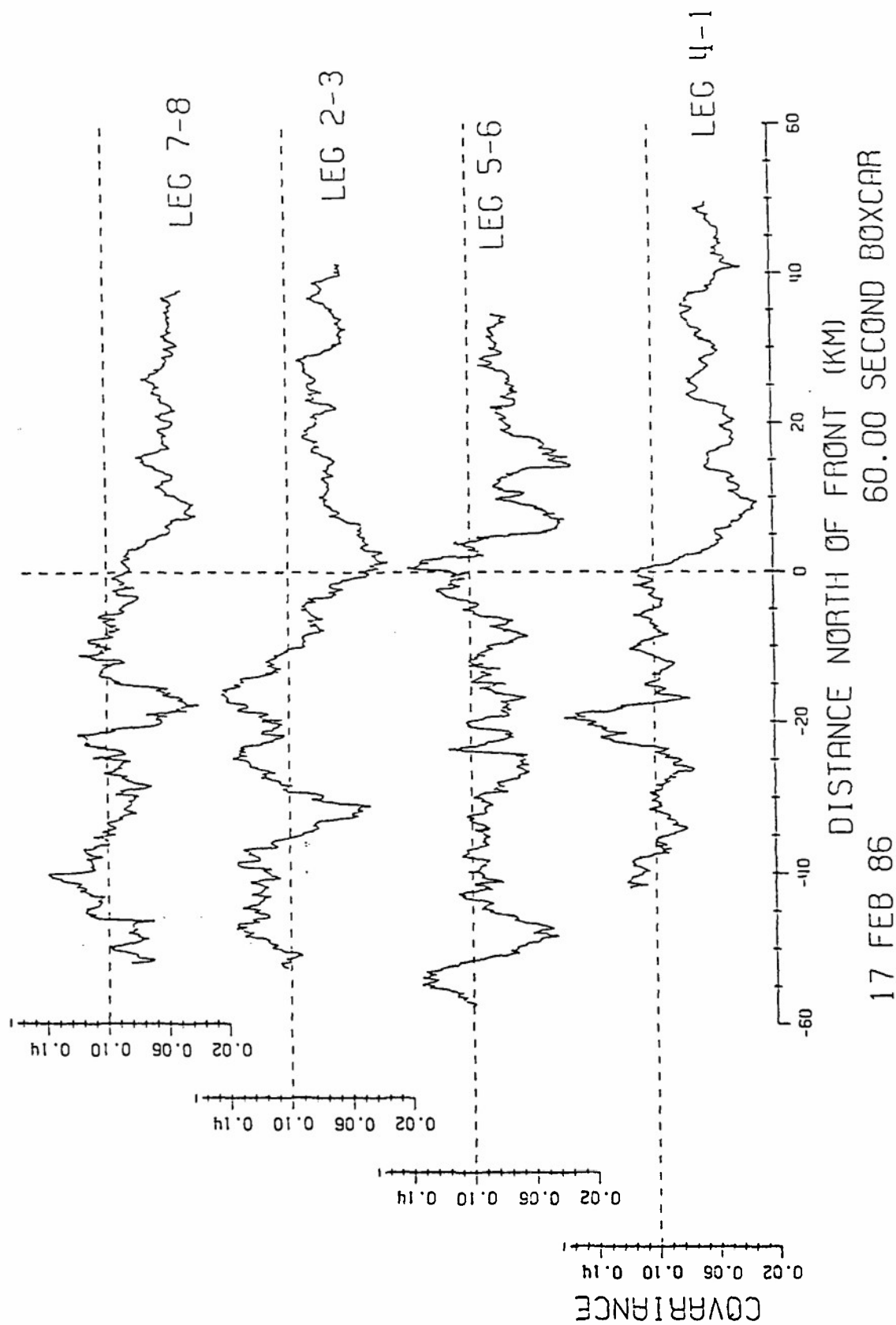


Fig. 22. The kinematic vertical specific humidity flux for all cross frontal legs on 17 February 1986.

FASINEX - NCAR ELECTRA N308D

U (m/s)

W (m/s)

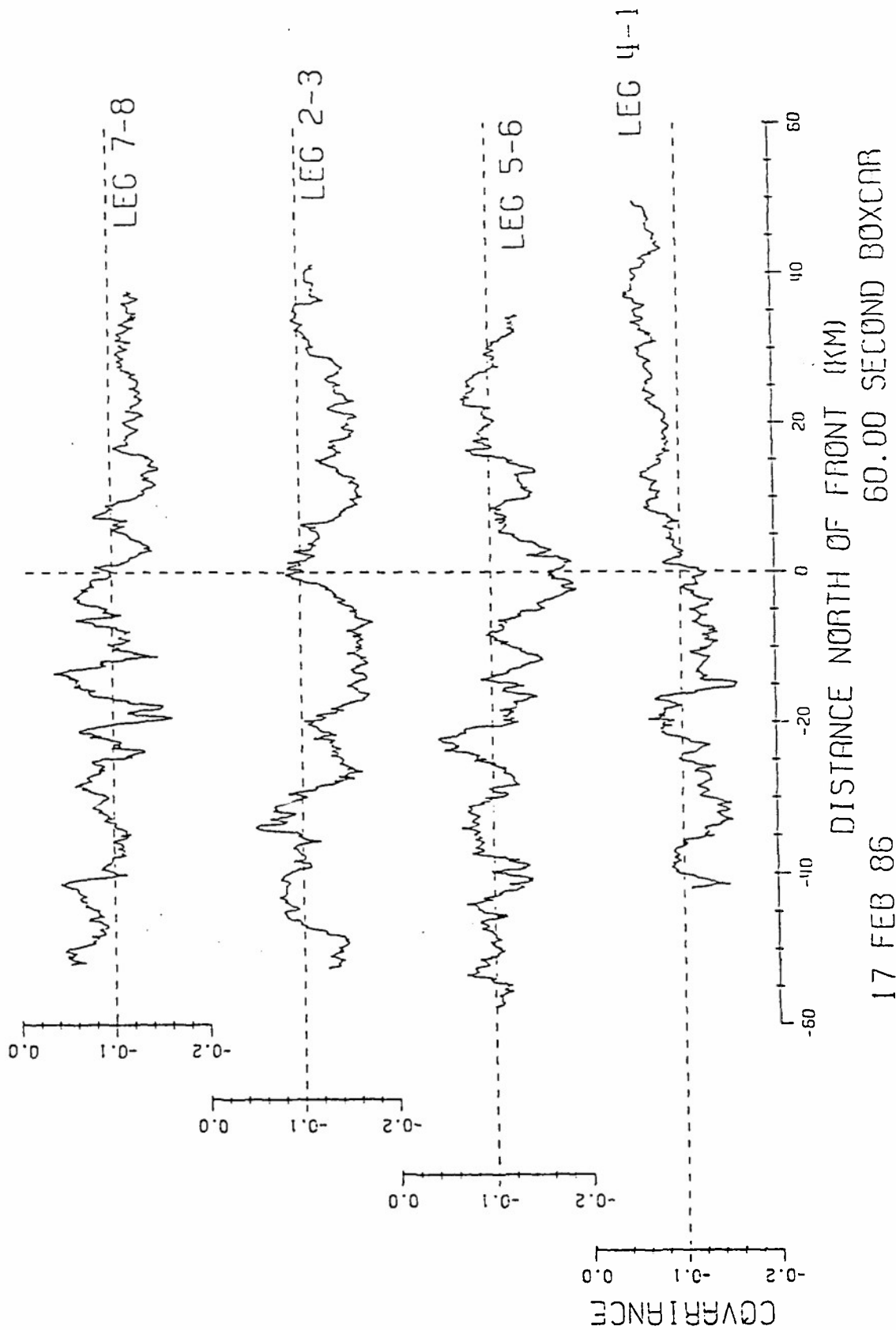
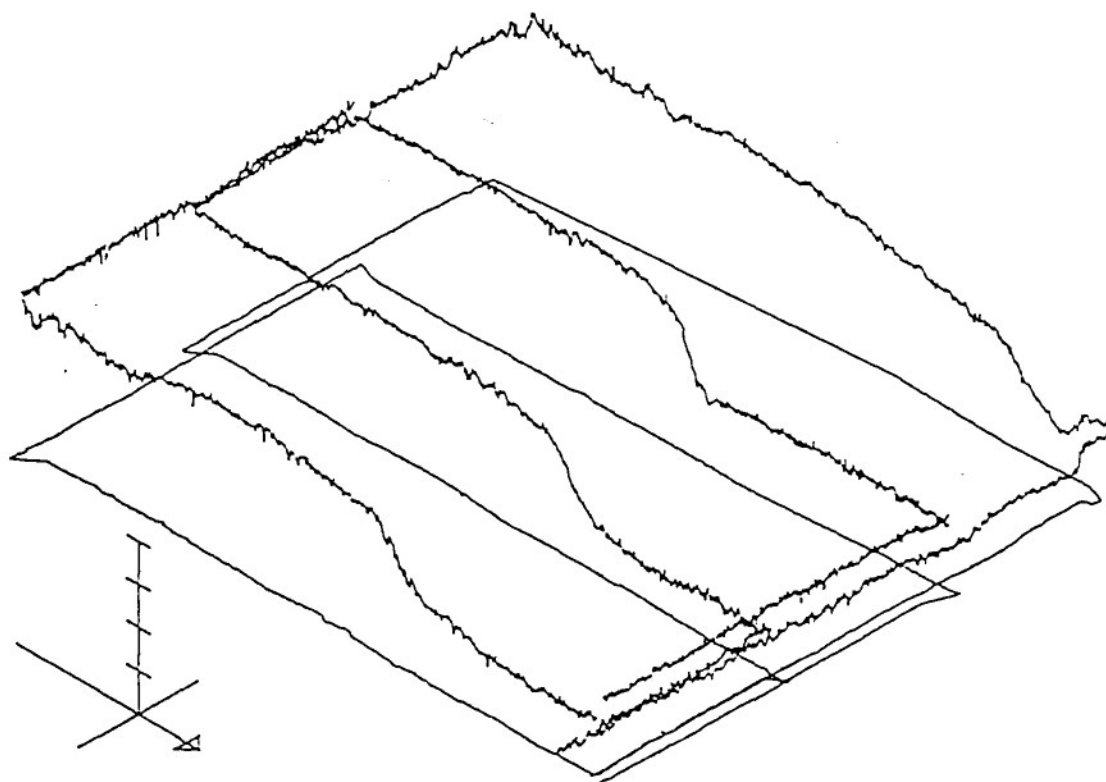


Fig. 23. The kinematic vertical momentum flux for all cross frontal legs on 17 February 1986.



Z AXIS MAX = 23.00
 Z AXIS MIN = 19.00
 Z INC = 1.00

Z MAX = 22.99
 Z MIN = 19.65

18 FEB 86
 SST (C)

Fig. 24. Three dimensional representation of sea surface temperature on 18 February 1986.

FASINEX - NCAR ELECTRA N308D
THETA (K)

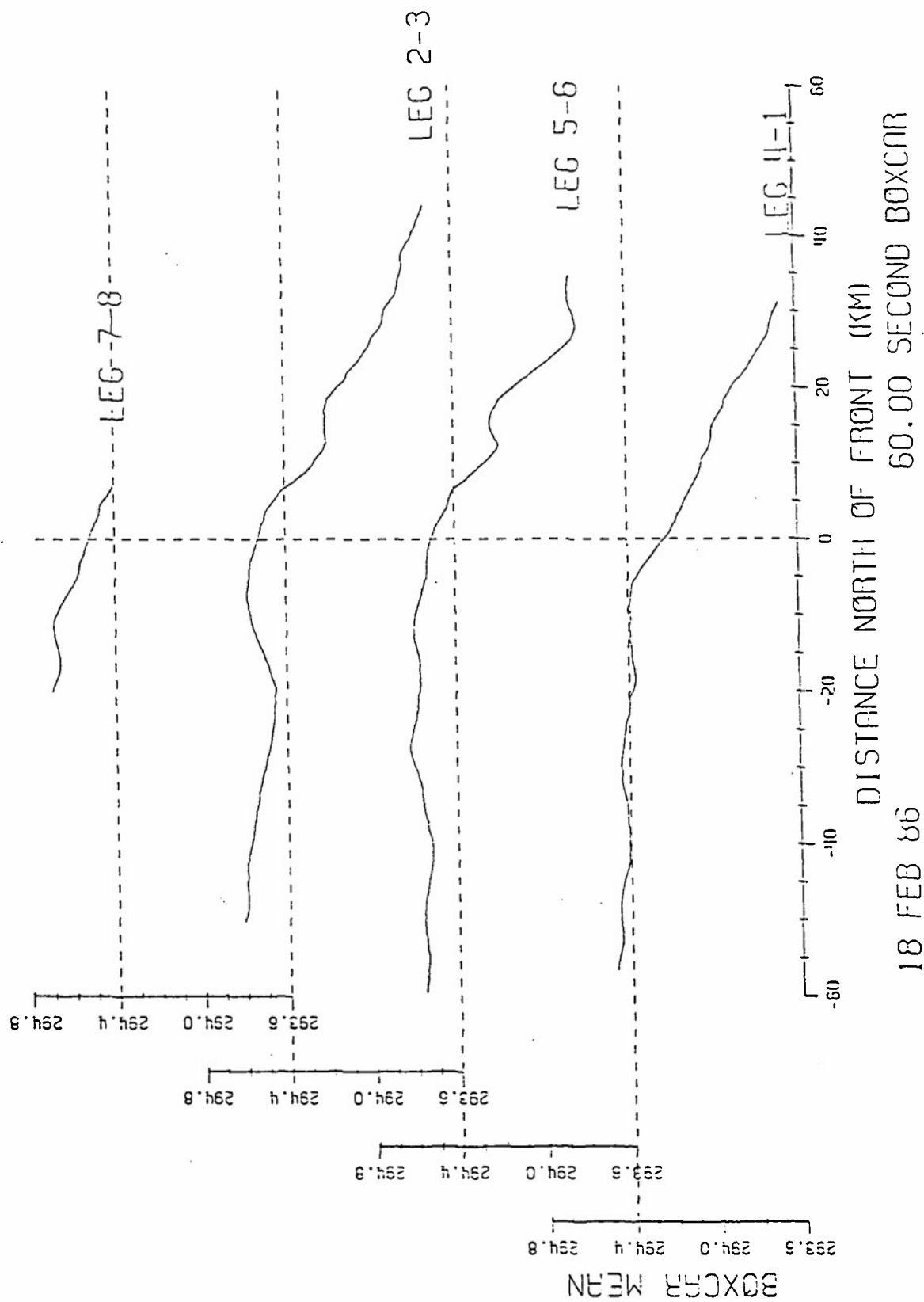


Fig. 25. Boxcar average of potential temperature for all cross frontal legs on 18 February 1986.

FASINEX - NCAR ELECTRA N308D
Q (g/kg)

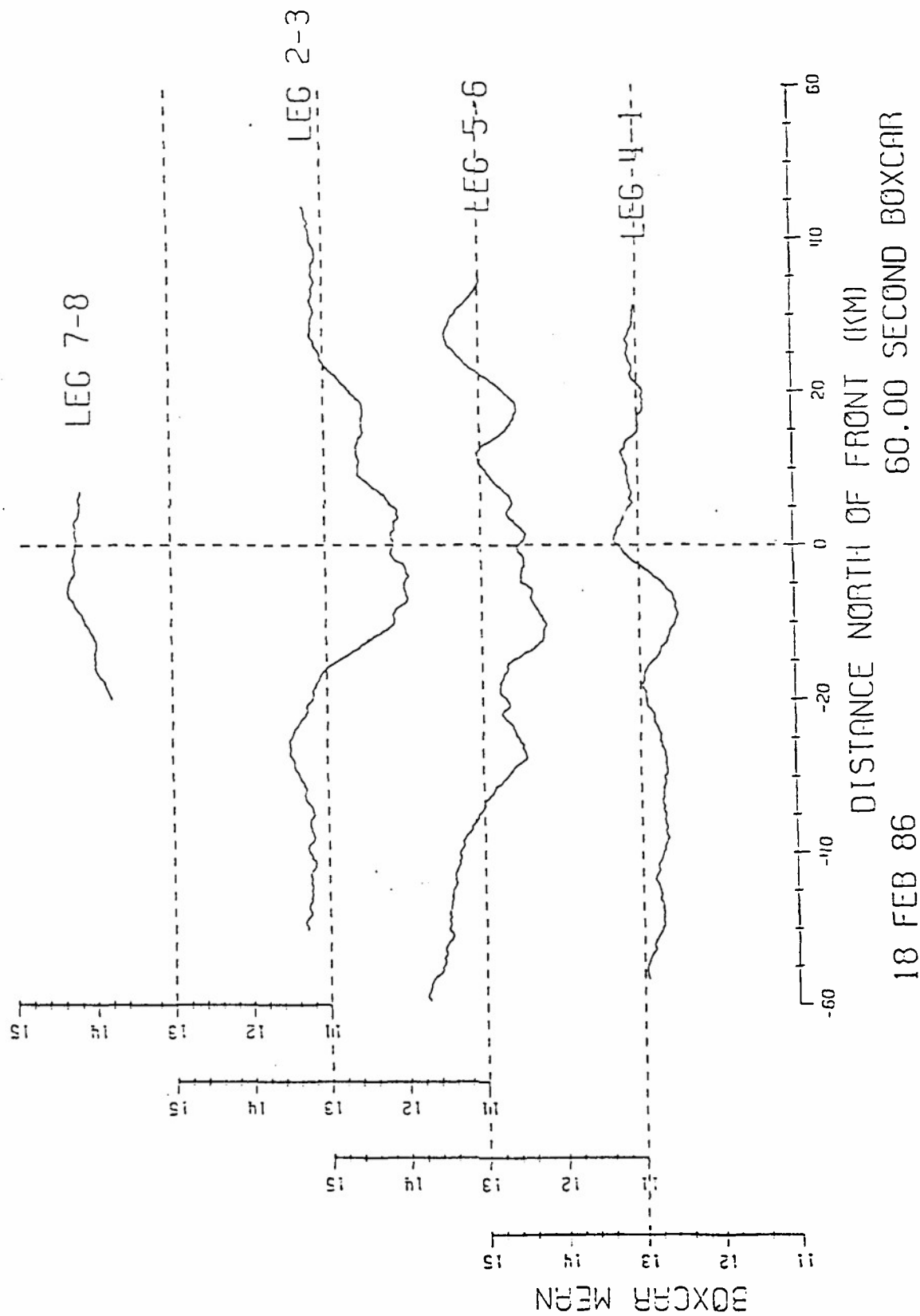


Fig. 26. Boxcar average of specific humidity for all cross frontal legs on 18 February 1986.

VARIANCE $\times 10^{-1}$

LEG 7-8

LEG 2-3

LEG 5-6

LEG 9-1

DISTANCE NORTH OF FRONT (KM)

60.00 SECOND BOXCAR

18 FEB 86

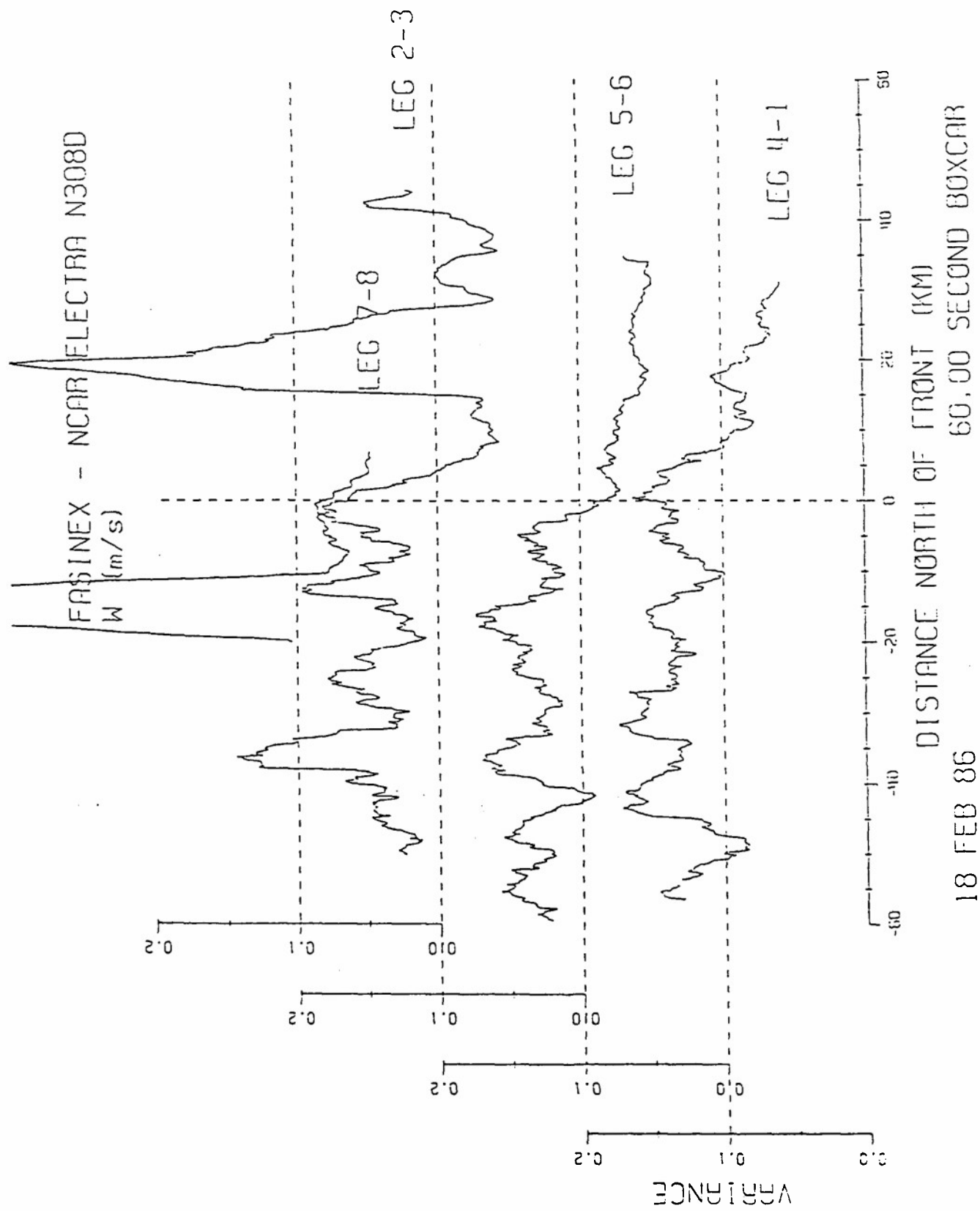


Fig. 28. Boxcar vertical velocity variance for all cross frontal legs on 18 February 1986.

FASINEX - NCAR ELECTRA N308D
Q (G/KG)

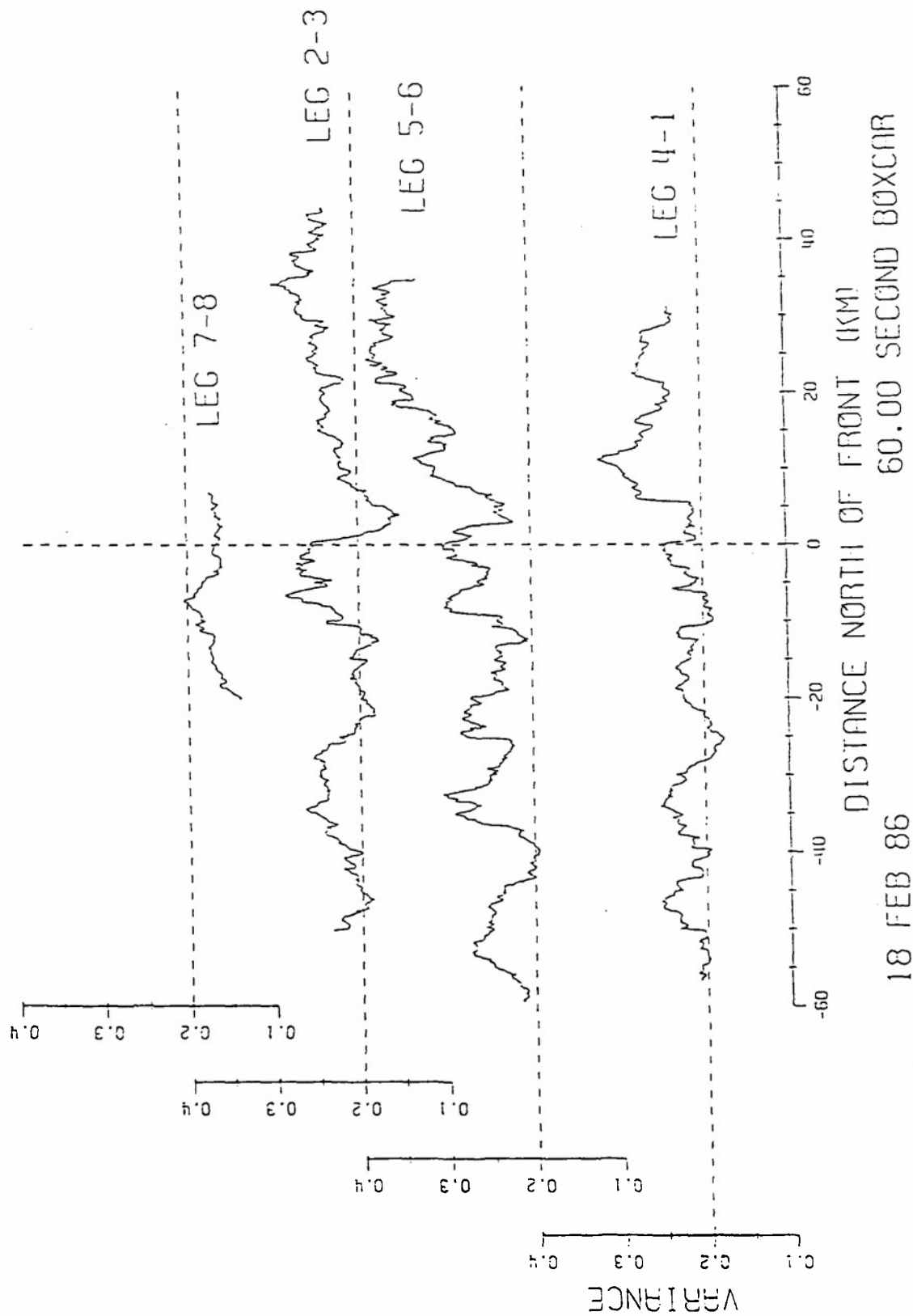


Fig. 29. Boxcar specific humidity variance for all cross frontal legs on 18 February 1986.

FASINEX - NCAR ELECTRA N308D
W (m/s) Q (g/kg)

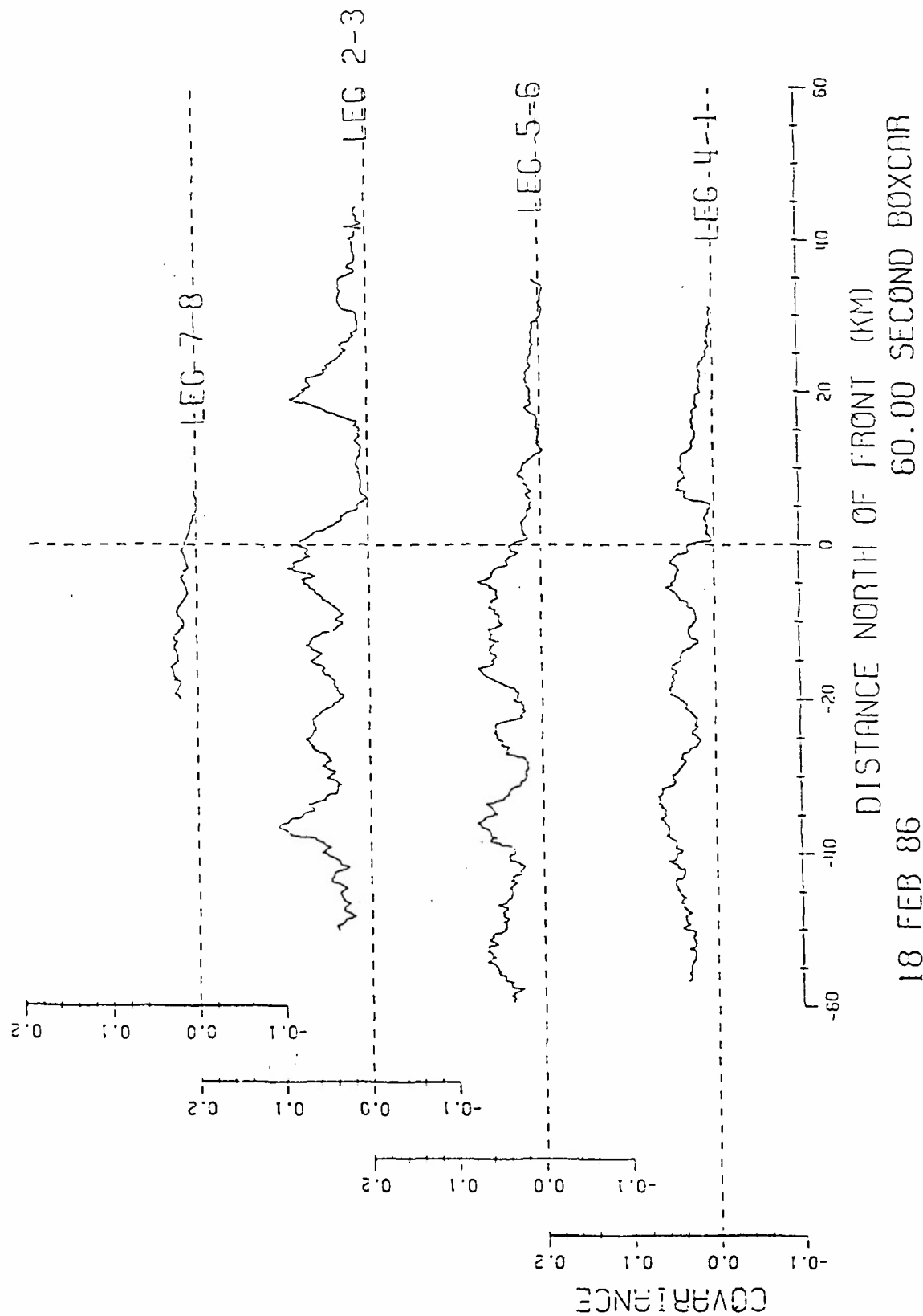


Fig. 31. The kinematic vertical specific humidity flux for all cross frontal legs on 18 February 1986.

FASINEX - NCAR ELECTRA N308D
W (m/s) THETA (K)

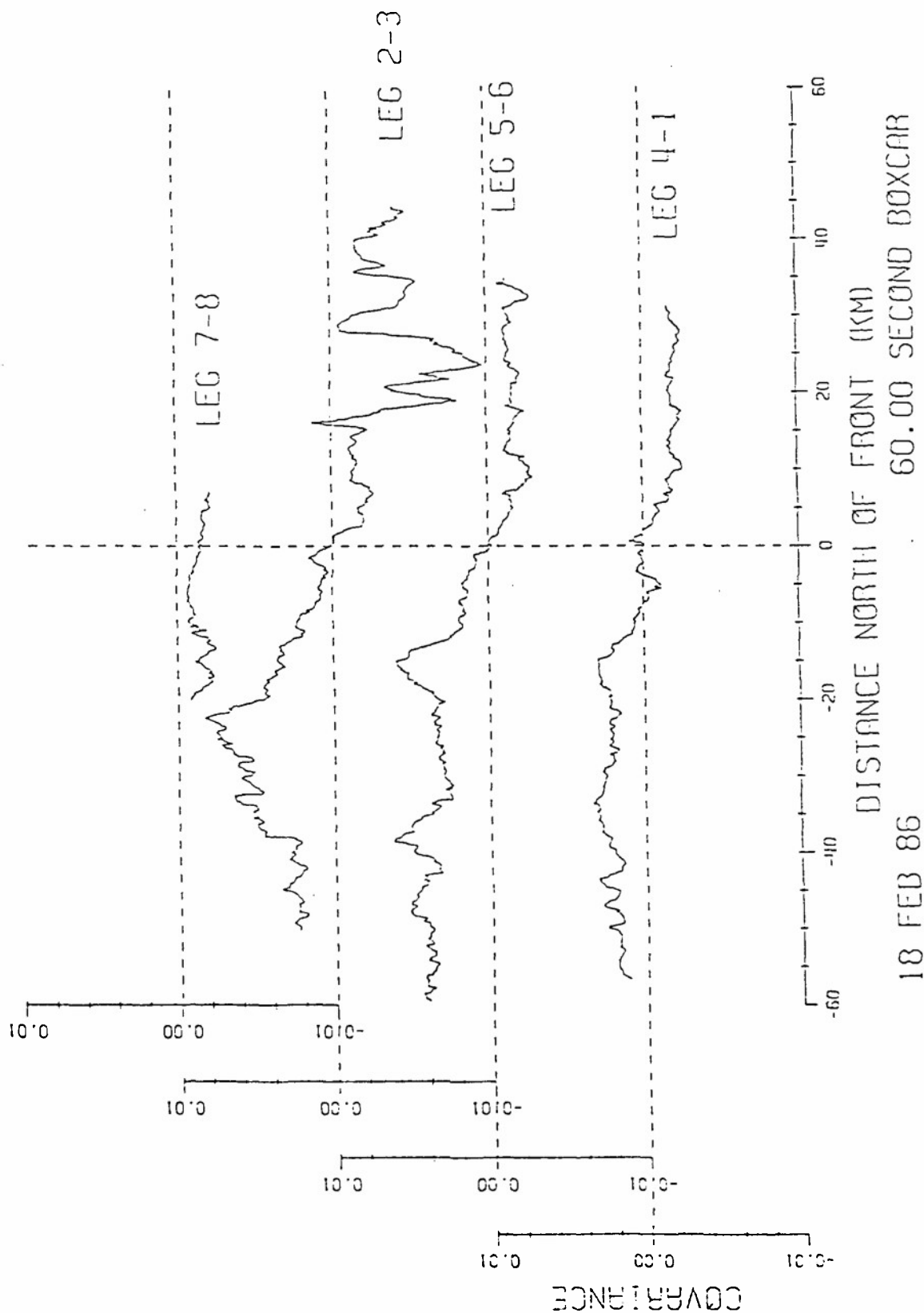


Fig. 30. The kinematic vertical heat flux for all cross frontal legs on 18 February 1986.

FASINEX - NCAR ELECTRA N308D
 U (m/s)
 W (m/s)

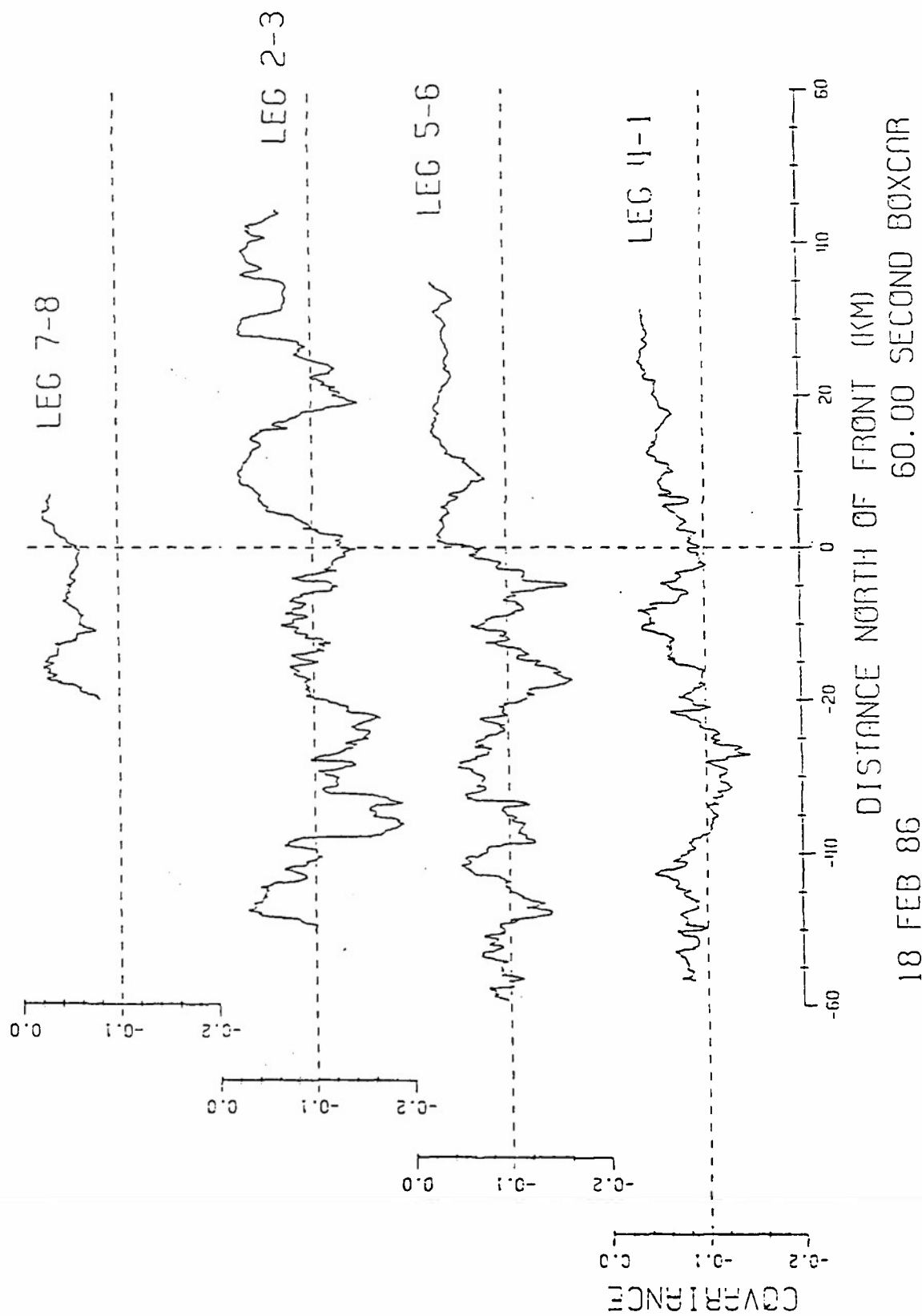


Fig. 32. The kinematic vertical momentum flux for all cross frontal legs on 18 February 1986.

FASINEX - NCAR ELECTRA N308D
W (m/s)
THETA (K)

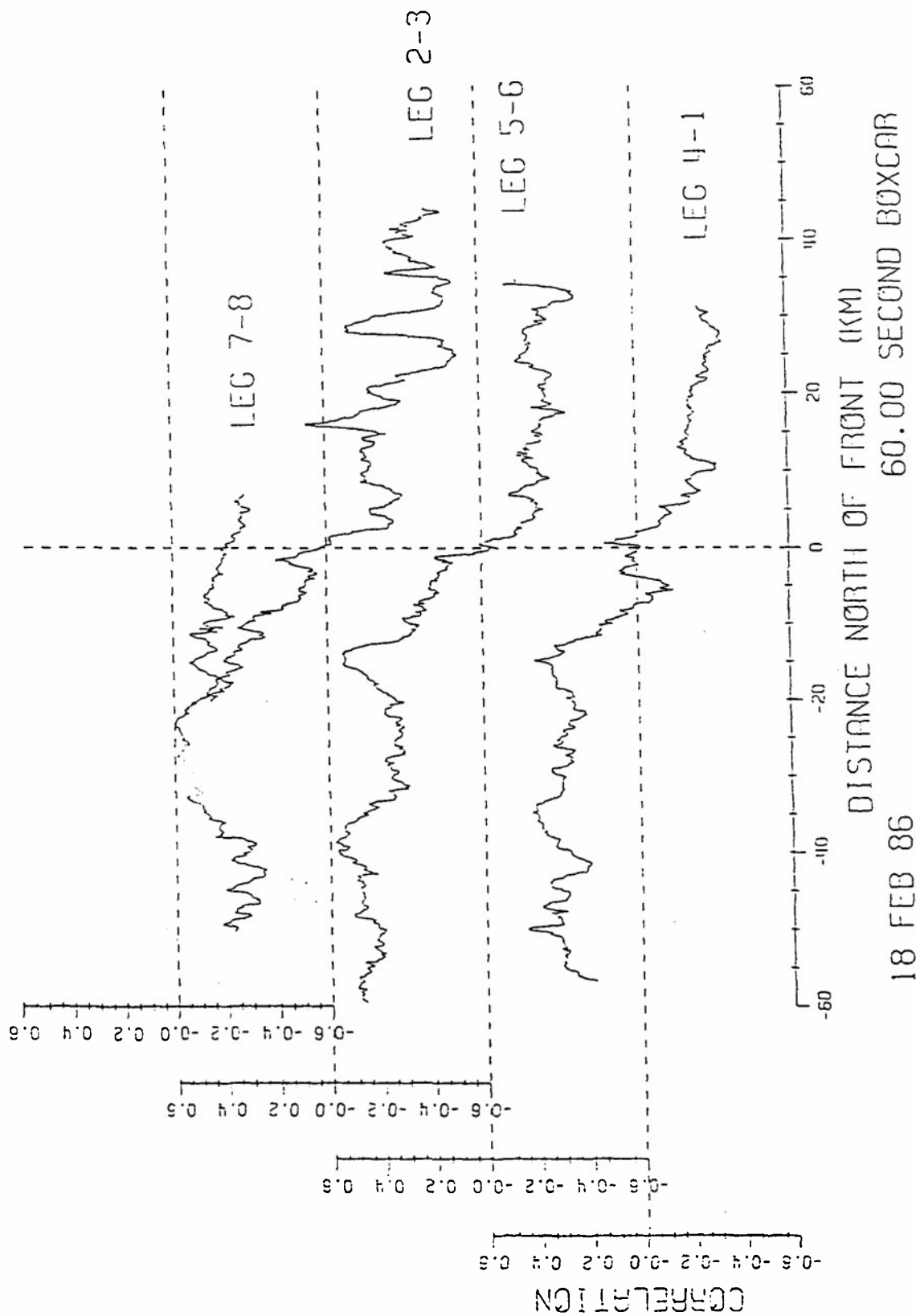


Fig. 33. Boxcar correlation between vertical velocity and potential temperature on 18 February 1986.